



Long-term experimental diagenesis of aragonitic biocarbonates: from organic matter loss to abiogenic calcite formation

Pablo Forjanes¹, María Simonet Roda², Martina Greiner², Erika Griesshaber², Nelson A. Lagos³, Sabino Veintemillas-Verdaguer⁴, José Manuel Astilleros^{1,5}, Lurdes Fernández-Díaz^{1,5}, Wolfgang W. Schmahl²

¹ Department of Mineralogy and Petrology, Universidad Complutense de Madrid, Madrid, 28040, Spain

² Department of Earth and Environmental Sciences, Ludwig-Maximilians-Universität, Munich, 80333, Germany

³ Centro de Investigación e Innovación para el Cambio Climático, Universidad Santo Tomás, Santiago, Chile

10 ⁴ Instituto de Ciencia de Materiales de Madrid (ICMM, CSIC), Madrid, 28049, Spain

⁵ Instituto de Geociencias (IGEO), (UCM, CSIC), Madrid, 28040, Spain

Correspondence to: Lurdes Fernández-Díaz (lfdz@geo.ucm.es) and Pablo Forjanes (pforjane@ucm.es)

15

Abstract. Carbonate biological hard tissues are valuable archives of environmental information. However, this information can be blurred or even completely lost as hard tissues undergo diagenetic alteration. This is more likely to occur in aragonitic skeletons because bioaragonite commonly transforms into calcite during diagenesis. For reliably using aragonitic skeletons as geochemical proxies, it is necessary to understand in depth the diagenetic alteration processes that they undergo. Several works have recently investigated the hydrothermal alteration of aragonitic hard tissues during short term experiments at high temperatures ($T > 160^{\circ}\text{C}$). In this study, we conduct long term (4 and 6 months) hydrothermal alteration experiments at 80°C using burial-like fluids. We document and evaluate the changes undergone by the outer and inner layers of *Arctica islandica* shell, the prismatic and nacreous layers of *Haliotis ovina* shell, and the skeleton of *Porites* sp. combining a variety of analytical tools (X-ray diffraction, thermogravimetry analysis, laser confocal microscopy, scanning electron microscopy, electron backscatter diffraction and atomic force microscopy). We demonstrate that this approach is the most adequate to trace subtle, diagenetic alteration-related changes in aragonitic biocarbonates. Furthermore, we unveil that the diagenetic alteration of aragonitic hard tissues is a complex multi-step process where major changes occur even at the low temperature used in this study and well before any aragonite into calcite transformation takes place. Alteration starts with biopolymer decomposition and concomitant generation of secondary porosity. These processes are followed by abiogenic aragonite precipitation that partially or totally obliterates the secondary porosity. Only afterwards any transformation of aragonite into calcite takes place. The kinetics of the alteration is highly dependent on primary microstructural features of the aragonitic biomineral. While the skeleton of *Porites* sp. remains virtually unaltered within the time span of the experiments, *Haliotis ovina* nacre undergoes extensive abiogenic aragonite precipitation, the outer and inner layers of *Arctica islandica* shell are significantly affected by aragonite transformation into calcite and this transformations extensive in the case of the prismatic layer of *Haliotis ovina*

20
25
30



35 shell. Our results suggest that most aragonitic fossil archives may be overprinted, even those free of clear diagenetic alteration signs. This finding may have major implications for the use of these archives as geochemical proxies.

Key words: Carbonates, Biominerals, Aragonite, Diagenesis, Diagenetic tracers: FE-SEM, EBSD, AFM.

1 Introduction

40

Calcium carbonate hard tissues are valuable geochemical proxies for deciphering past climate dynamics and environmental change. However, the greatest challenge that these biological archives face lies in their capacity to retain their pristine signature after the death of the calcifying organism, since from this moment, the skeletons become highly prone to alteration. The original microstructure and chemical composition of the skeleton can become partially, in the best case, to totally obliterated, and so
45 does the environment-derived information recorded in it (Brand, 1989; Swart, 2015; Casella et al., 2018, Pederson 2019a, 2019b, 2020).

Biocarbonate hard tissues are composites of biopolymers and calcium carbonate mineral phases (mostly calcite and/or aragonite, rarely and much less abundantly vaterite) (Weiner and Dove, 2003). The alteration of biocarbonate hard tissues and
50 the overprint undergone by their features are influenced by both external, environment-related, and internal, archive-related, factors. Main external factors are: alteration time, the degree of geochemical disequilibrium with the environment, the physicochemical conditions in the depositional environment, the porosity and permeability of the sediments, the chemical composition of the pore fluids and the fluid-rock ratio, among others (Pederson et al., 2019a, 2019b, 2020). On the other hand, some internal factors that influence the alteration kinetics of the calcium carbonate skeletons are the concerned carbonate
55 phase, the original microstructure and texture of the mineral component, its fabric, the amount and distribution of the organic matter within the composite hard tissue, etc. (Gaffey 1988; Gaffey et al., 1991, Casella et al., 2018, Pederson et al., 2020). At the conditions that reign in natural diagenetic environments calcite is the stable calcium carbonate polymorph while aragonite is a more soluble, thermodynamically metastable phase (Plummer and Mackenzie, 1974; Plummer and Busenberg, 1982; Sass et al., 1983; Walter and Morse, 1984; Bischoff et al., 1987, 1993; Redfern et al., 1989; Navrotsky, 2004; Morse et al., 2007;
60 Gebauer et al., 2008, Radha et al., 2010; Gebauer and Cölfen, 2011; Radha and Navrotsky, 2013). In the presence of an aqueous phase, aragonite crystals can transform into calcite through a coupled dissolution-crystallization reaction whose progress is driven by the difference in solubility between both phases and facilitated by the generation of porosity (Berner, 1975; Bischoff, 1969; Bischoff, 1968; Fyfe and Bischoff, 1965; Cardew and Davey, 1985; Mucci et al., 1989; Putnis and Putnis, 2007; Putnis, 2009, Ruiz-Agudo et al., 2014; Sun et al., 2015). The result of this dissolution-crystallization reaction is the formation of
65 calcite after aragonite pseudomorphs that consist of blocky calcite crystals (Perdikouri et al., 2008, 2011, 2013).



The metastable nature of aragonite explains that aragonitic skeletons have a lower potential of becoming preserved in the geologic record, relative to their calcitic counterparts (James et al., 2005; Cherns and Wright, 2011; Cherns et al., 2011, Janiszewska et al., 2018; Wright et al., 2003; Wright and Cherns 2004). Lowenstam (1954) and Hallam and O'Hara (1962) estimated that, during diagenesis, most aragonitic carbonates would be replaced by calcite within a few to thousands of years. However, under low-temperature regimes, in shallow enriched in organic matter environments, the transformation of aragonite into calcite is precluded and the progress of diagenetic alteration is restricted to its very first stages (Hall and Kennedy, 1967; Seuss et al. 2009; Janiszewska et al., 2018). The resulting structural and chemical changes between the pristine and altered skeletons are then very subtle and difficult to trace. In this work we aim to disclose the subtle microstructural and chemical changes undergone by aragonitic hard tissues during low-temperature/long-time hydrothermal alteration. We conducted long-term (4 and 6 months) hydrothermal alteration experiments at 80°C with burial-mimicking Mg-rich waters. Aiming to understand the influence of bioaragonite architecture in the kinetics of hydrothermal alteration we investigated the alteration response of three very different biocarbonate skeletons: (i) the granular aragonite that forms the shell of the bivalve *Arctica islandica*, (ii) the prismatic and columnar nacreous aragonite that comprises the shell of the gastropod *Haliotis ovina* and (iii) the acicular, fibrous aragonite that builds up the skeleton of the coral *Porites* sp. By comparing the hydrothermal overprint undergone by these microstructures after prolonged alteration at 80°C (this study) and after much shorter alteration at 175 °C (Casella et al., 2018) we better identify early hydrothermal alterations steps and improve our understanding of the role of temperature and time in the progress of alteration overprint. This study demonstrates that a combination of analytical tools and evaluation techniques (TGA and XRD measurements, Rietveld analysis of XRD data, EBSD measurements and grain size statistical evaluation, laser confocal microscopy, FE-SEM and AFM imaging) provides the ideal set of data to pinpoint the structural changes caused by the hydrothermal and/or diagenetic alteration of biological hard tissues, even the subtle, difficult to address ones that mark the very first steps of biocarbonate microstructural reorganization.

2 Material and Methods

2.1 Materials

90

Three aragonitic hard tissues from animals with very different microstructures were chosen for this study. Shells of the modern bivalve *Arctica islandica* were collected from Loch Etive in Scotland (United Kingdom). Adult specimens of the gastropod *Haliotis ovina* were obtained at Heron Island in Queensland (Australia). Samples of the scleractinian coral *Porites* sp. were collected at Moorea, French Polynesia (France).

95 2.2 Methods

2.2.1 Hydrothermal Alteration Experiments



For alteration experiments, pieces of the hard tissues were cut into slices with a diamond 6-inch saw (Hi-Tech-Diamond) and cut subsequently into three rectangular 2 cm x 1 cm fragments (Fig. A1). All three segments were hydrothermally altered.
100 Hydrothermal alteration experiments were carried out mimicking diagenetic conditions regarding fluid temperature and composition. The used fluid composition (100 mM NaCl + 10 mM MgCl₂) simulates the fluid present at a burial diagenetic realm. The composition of the fluid was identical to that previously used by Casella et al., (2017, 2018) and Pederson et al., (2019a; 2019b; 2020) in their hydrothermal alteration experiments.

105 For all alteration experiments, 3 pieces of the pristine skeletons of modern *Arctica islandica*, *Porites* sp. and *Haliotis ovina* were placed into a polytetrafluoroethylene (PTFE) vessel together with 10 mL of the Mg-rich burial aqueous solution. The PTFE vessels were then sealed with a PTFE cover and inserted into stainless-steel autoclaves, which were subsequently sealed, and kept in an oven at 80°C for 4 and 6 months. After hydrothermal alteration, the autoclaves were recovered from the oven, cooled down at room temperature (20°C) and opened. The recovered altered samples were dried overnight at 40°C in a furnace.
110 Subsequently, the samples were prepared for further analysis. For all the hydrothermal experiments it was ensured that the shell pieces selected for alteration were taken from the same valve to avoid differences in the alteration caused by metabolic effects.

2.2.2 Structural Hard Tissue Characterization

X-ray diffraction (XRD) and Rietveld analysis

115 One of the three pieces of every altered sample was crushed in an agate mortar and measured with powder X-ray diffraction (XRD) for phase composition evaluation. The analysis was performed using Cu-K α 1 radiation in reflection geometry on a General Electric Inspection Technologies XRD3003 X-ray diffractometer with an incident-beam Ge111 focussing monochromator and a Meteor position-sensitive detector (GE Inspection Technology GmbH). The obtained XRD data were
120 evaluated with Rietveld analysis, using the software FULLPROF (Rodriguez-Carvajal, 2001) and the CIF structural data from Markgraf and Reeder (1985) for calcite and from Jarosch and Heger (1986) for aragonite, from the Crystallography Open Database (COD 2017). The above-described data evaluation procedure was applied to all pristine as well as altered samples.

Thermal Gravimetric Analysis (TGA)

125 The sample that was used for XRD measurements was recovered from the XRD holder and was further used for TGA measurements for the determination of organic matter content within the pristine and altered sample. TGA measurements were conducted with a Q500 TGA. The samples were heated from room temperature to 1000°C at a constant rate of 5°C per minute in a flowing-air atmosphere. 25 mg of powder of every sample were used for TGA analysis.

130



2.2.3 Imaging Techniques

Laser Confocal Microscopy

Overview images for the visualization of the different microstructures within a shell or skeletal element were taken with a
135 Keyence 3D laser scanning confocal microscope (VK-X1000 series). Shell and skeleton segments were embedded in epoxy
resin and polished down with eight sequential polishing steps for obtaining a highly even sample surface. Laser confocal
microscopy imaging was conducted on uncoated samples.

Atomic Force Microscopy (AFM)

140

The sub-micrometre and nanometre structure of the shells and skeletal elements was scanned with AFM. AFM imaging was
done in non-coated, epoxy-embedded and highly polished sample surfaces. Samples were imaged in contact mode with a JPK
NanoWizard II AFM using silicon nitride cantilevers. Scans of lateral and vertical deflection traces were analysed with the
NanoWizard® IP image processing software by using the “gold” scale for colour. The lateral and vertical deflection traces are
145 the result of the interaction between the cantilever tip and the sample surface. Height traces were used to generate 3D models
of the nanoscale topography of some of the samples.

FE-SEM imaging and EBSD measurements

150 To visualize major microstructural elements in the pristine and the altered samples, the aragonitic hard tissues were imaged
with FE-SEM and analyzed with EBSD. The remaining piece of the altered samples, together with pristine skeletons, were
embedded into epoxy resin and polished with several mechanical grinding and polishing steps down to a grain size of 1 µm.
Subsequently, the samples were polished with an alumina (particle size ~0.06 µm) containing suspension in a vibratory
polisher (VibroMet 2; Buehler) for 2 hours. For EBSD measurements the samples were coated with 5 to 6 nm of carbon, for
155 FE-SEM imaging, additionally with 8 to 10 nm of Pt/Pd.

FE-SEM imaging and EBSD measurements were carried out in a Hitachi SU5000 field emission SEM, equipped with an
Nordlys Oxford EBSD detector. The SEM was operated at 20 Kv and the Kikuchi diffraction patterns were indexed with the
Oxford Instruments AZTec and CHANNEL 5 HKL software (Schmidt and Olesen, 1989; Randle, 2000). Information obtained
160 from EBSD measurements is presented here as band contrast measurement images and as colour-coded crystal orientation
maps with their corresponding pole figures; the latter giving either individual data points or, in the contoured version, the
strength of the clustering of poles (Half width of 5° and cluster size of 3°).



165 EBSD band contrast gives the signal strength of the EBSD-Kikuchi diffraction pattern and is displayed as a grey-scale
component in a map. The strength of the EBSD signal is high when a crystal is detected (bright in the map), whereas it is weak
or absent when a polymer, such as organic matter or epoxy resin, is scanned (dark/black on the map). Crystal co-orientation
statistics are derived from Kikuchi diffraction patterns measured at each image pixel of an EBSD map. Crystal co-orientation
is given by the MUD value (multiple of uniform (random) distribution). A high MUD indicates high crystal co-orientation,
while low MUD values reflect low to random crystallite or/and mineral unit co-orientation. Pole figures are stereographic
170 projections of the orientations of crystallographic axes or plane normals measured at all pixels of an EBSD map.

The term texture relates to the distribution of crystal orientations within a material and is illustrated by pole figures, showing
either colour-coded orientation data or contoured versions of density distributions of c- and a*-axes poles. A fibre texture or
axial texture is present when the measured orientations have a one-dimensional orientation order. For brachiopod shell calcite
175 usually the c-axes of the individual crystals are co-oriented, showing a cluster concentrated around one particular direction in
the {001} (= c-axis) pole figure, whereas the {100} (= a*-axes) scatter in orientation around the great circle perpendicular to
the c-axis. A three-dimensional texture or three dimensional orientational order is present when all crystallographic axes in the
investigated map are co-oriented, such that there is a concentrated cluster of data points around one particular direction in the
c-axes pole figure but also distinct clustering on the great circle perpendicular to this direction in the a*-axes pole figure. Since,
180 for calcite, the c-axis is a unique direction and bears the $3\bar{2}$ -symmetry axis, there are six maxima in the a*-axis pole figure.
However, only three of those are usually visible in the pole figure because data of only one hemisphere of the stereographic
projection are displayed. The term microstructure refers to the sum of grains, their sizes, morphologies, modes of interlinkage,
co- and misorientations and is shown with coloured EBSD maps. Similar colours visualize similar crystal orientations, different
colours indicate differences in crystal orientation.

185

Grain area/size statistical evaluation

EBSD measurements allow us to distinguish between individual grains and, hence, to obtain grain related parameters such as
grain area and grain boundaries. A grain in an EBSD map is defined as a region that is completely surrounded by boundaries
190 across which the misorientation angle relative to the neighbouring grains is larger than a critical value. In this study we use a
critical misorientation value of 2° . The latter was determined empirically and is appropriate for carbonate biological hard
tissues (Griesshaber et al., 2013). To evaluate grain size distributions, we chose grain clusters with a class width of $0.10 \mu\text{m}^2$
for aragonite nacre tablets and $0.15 \mu\text{m}^2$ for the other aragonitic microstructures. In this study we plotted the relative frequency
of every cluster with respect to the total amount of grains (%) relative to grain area/grain size (μm^2).

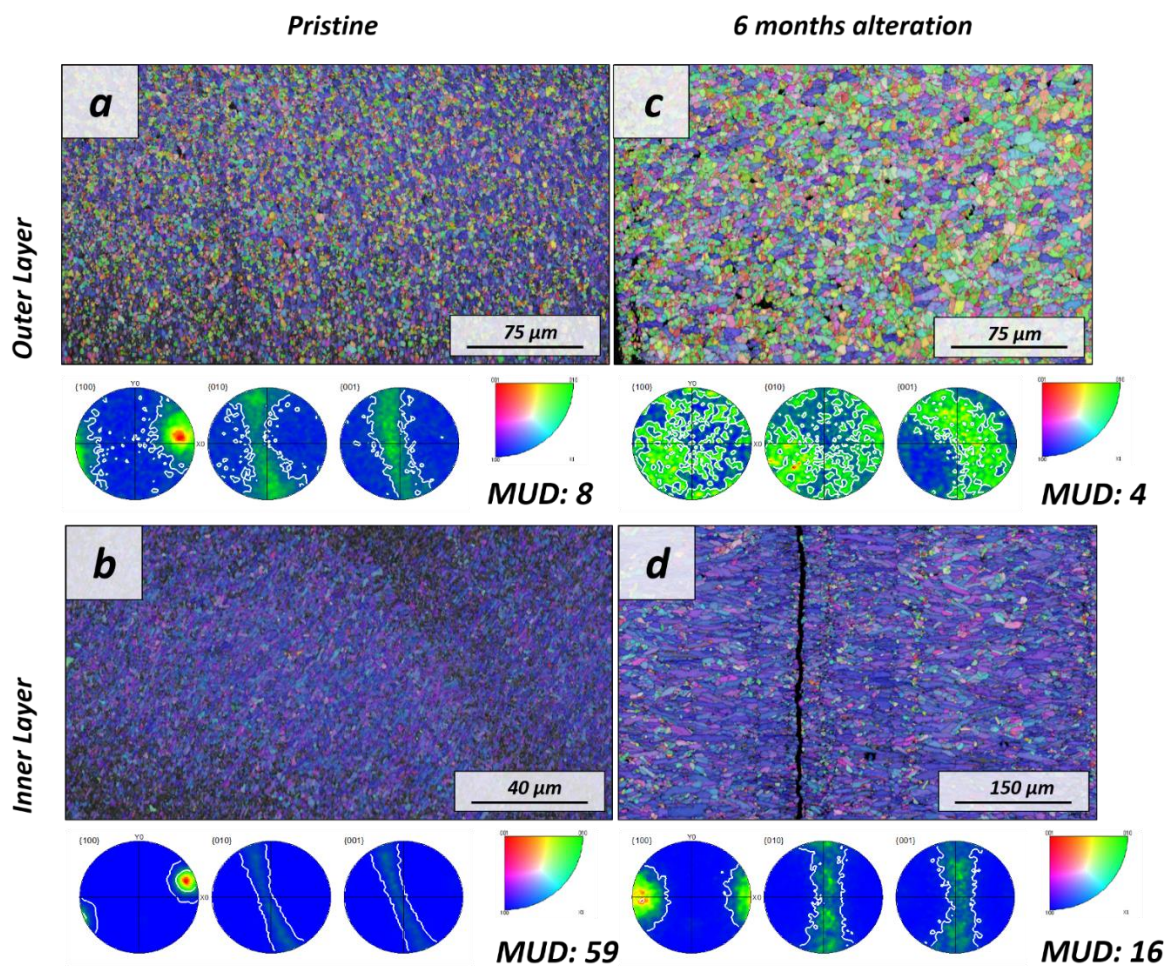
195

3 Results



3.1 The pristine microstructure of *Arctica islandica*, *Haliotis ovina* and *Porites* sp. skeletons.

- 200 The pristine skeletons of *Arctica islandica*, *Haliotis ovina* and *Porites* sp. consist entirely of aragonite according to XRD measurements and Rietveld analysis (Fig. A2 and A4 from Casella et al., 2018) and have an organic matter content that varies significantly for the different species. Organic matter concentration in the investigated hard tissues was determined with TGA analyses (Fig. A3).
- 205 The shell of the bivalve *Arctica islandica* is comprised of irregularly shaped micrometre-sized aragonite crystals which are interconnected by a network of biopolymer fibrils (Casella et al., 2017). Annual growth lines are frequent (Fig. A4 and A5). Aragonite crystals are unstructured and show a poor co-orientation strength according to EBSD measurements and data analysis (MUD = 8). This is the case for the outer region of the shell next to seawater. Contrarily, the crystals which constitute the innermost layer of the skeleton closer to the soft tissue of the animal, have a crossed lamellar microstructural arrangement,
- 210 with higher MUD values (59) (Fig. 1 and A6). Despite having a densely packed aragonitic microstructure, the pristine skeleton of *Arctica islandica* contains primary porosity. This porosity is more abundant in the outer regions of the shell and decreases towards the inner region (Fig. A4 and A5). TGA analysis of the pristine shell of *Arctica islandica* show that the amount of organics in the shell varies between 1.8 wt. % in the inner shell portion and 2.2 wt. % in the outer shell portion (Fig. A3). Despite the differences in shell microstructure, aragonite nanostructure is relatively homogeneous throughout the pristine
- 215 *Arctica islandica* shell. AFM images show that aragonite has a slightly rough surface made up of spherical aragonite subunits down to 0.1 μm in diameter (yellow star in Fig. 2).



220 **Figure 1.** EBSD colour-coded orientation maps with their corresponding pole figures depicting aragonite microstructure and texture in: (a-b) pristine and (c-d) altered shells of the bivalve *Arctica islandica*. The strength of crystal co-orientation is given with the MUD value for the relevant EBSD scan, which is shown for each EBSD measurement. Even though that at the applied hydrothermal alteration new abiogenic calcite formation does not yet take place, the strong decrease in MUD values between the pristine and the altered samples indicates reorganization of the microstructure through new, abiogenic, aragonite formation.

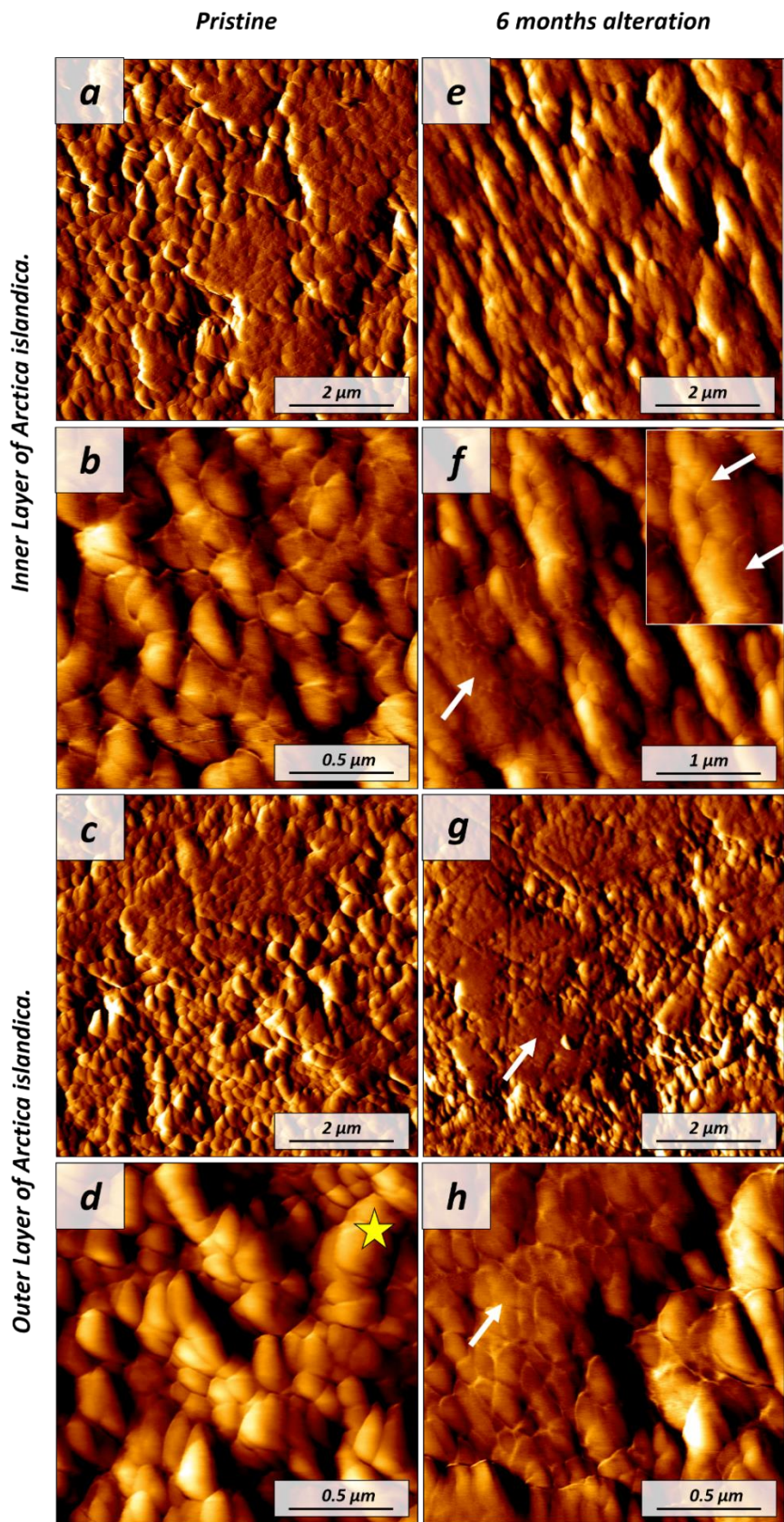
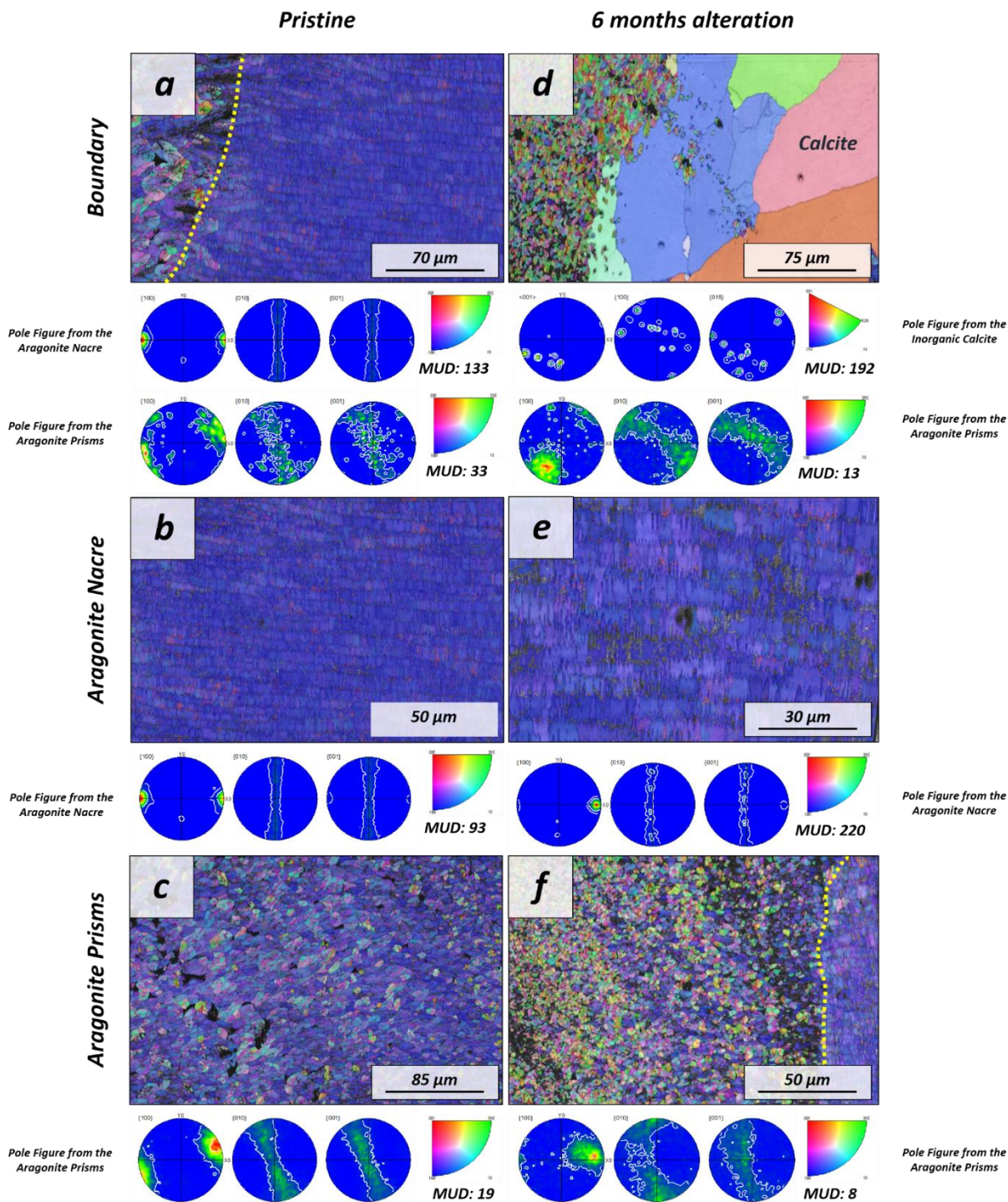




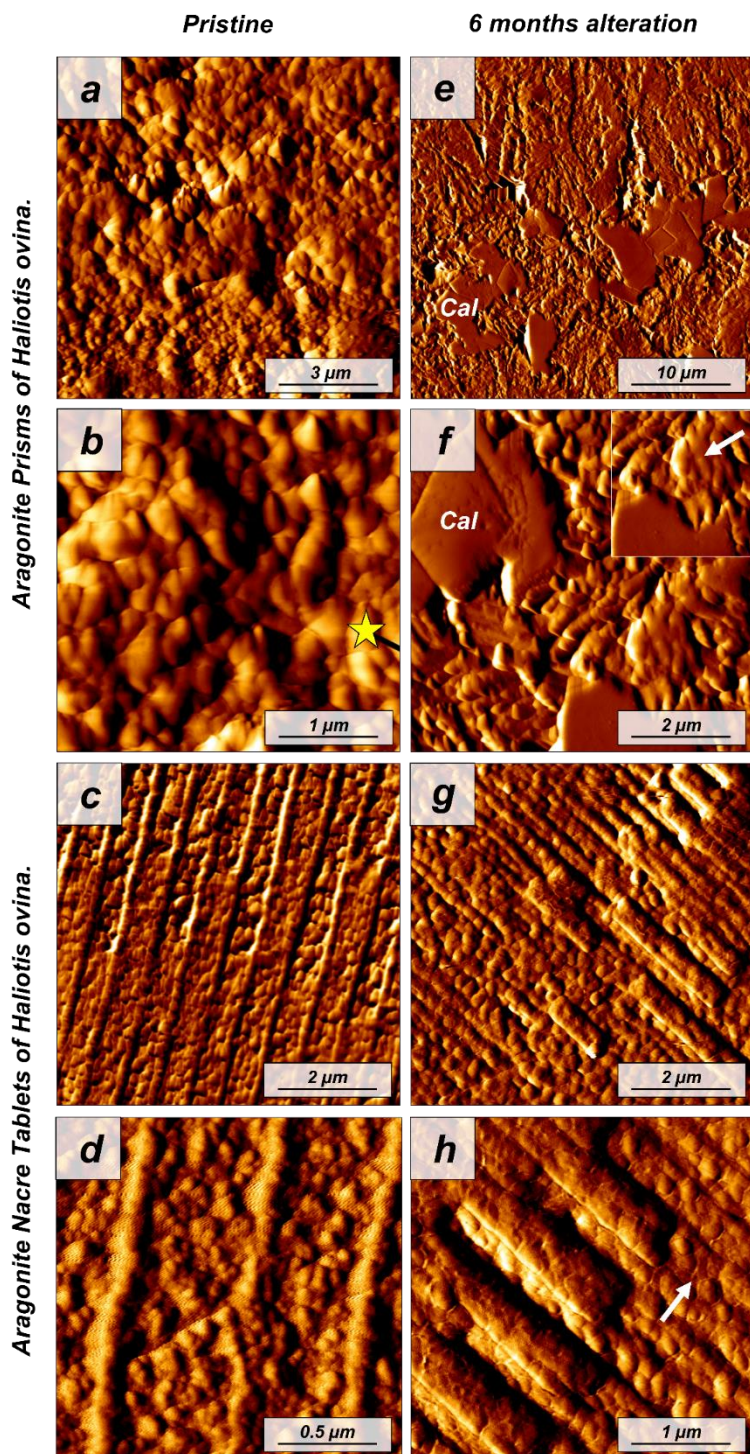
Figure 2. Vertical deflection AFM images of: (a-d) pristine and (e-h) altered shells of the bivalve *Arctica islandica*. Pristine shells of *Arctica islandica* are composed of two aragonitic layers formed by aragonitic subunits up to 0.1 micrometres in size (yellow star in Fig. 2d). Hydrothermal alteration induces amalgamation of the subunits (white arrows in Figs. 2e to 2h).

The pristine shell of the gastropod *Haliotis ovina* shows two microstructural arrangements. The outer layer closer to the seawater is composed of aragonite prisms while the inner layer closer to the soft tissue of the animal is composed of aragonitic nacre tablets (Fig. A7 and A8), which are arranged in columns. The aragonite prisms have an irregular shape and show a gradation in size, such that the smaller crystals are in the outermost regions of the shell, in contact with the seawater, and the largest aragonite prisms are close to or at the transition with the nacre (Fig. A9a). The nacre tablets, on the other hand, have an average thickness of 430 to 500 nm (Fig. A9b). There is a very sharp boundary between the two microstructures. Aragonitic nacre represents about 80 to 85% of the shell of *Haliotis ovina*, while the aragonitic prisms represent the remaining 15 to 20%. EBSD analyses demonstrate that the aragonitic nacre is highly co-oriented, with a MUD value close to 100. In contrast, crystals that form the aragonitic prisms show a lower crystal co-orientation. MUD values scatter between 19 and 31 (Fig. 3 and A10). TGA analysis of the pristine shell of *Haliotis ovina* gives that the amount of organics in the shell is 3.1 wt. %. The nanostructures of the two microstructural arrangements of pristine *Haliotis ovina* are depicted in Fig. 4. Aragonite prisms have a rough surface composed of up to 0.3 μm aragonite subunits (yellow star in Fig. 4b). Aragonite nacre tablets are formed by smaller aragonitic subunits separated by linear continuous divisions, the sites where the organic matter is concentrated. A 3D model of the nacre surface derived from height AFM measurements is shown in Fig. 5 and shows that this microstructure has a topography in which the divisions between the different tablets, that is, the place where the organic matter is concentrated, stands out topographically (30 nm on average) above the mineralized areas.



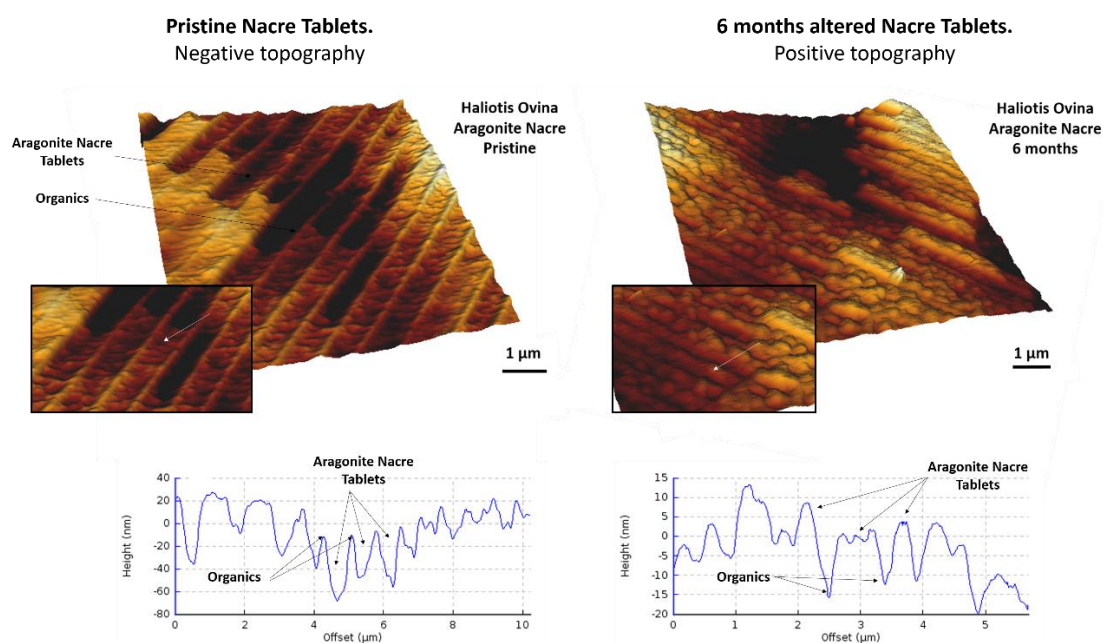


255 **Figure 3.** EBSD colour-coded orientation maps with their corresponding pole figures depicting the microstructure and texture of biogenic aragonite of the (a-c) pristine and (d-f) altered shells of the gastropod *Haliotis ovina*. The strength of crystal co-orientation is given with the MUD value, which is shown for each EBSD scan. Hydrothermal alteration of *Haliotis ovina* induces the replacement of large parts of the prismatic aragonite by non-biogenic calcite concomitantly to a decrease of the MUD value of the untransformed aragonite prisms. Though the nacreous layer is not replaced by calcite, its MUD value increases from 93 to 220.



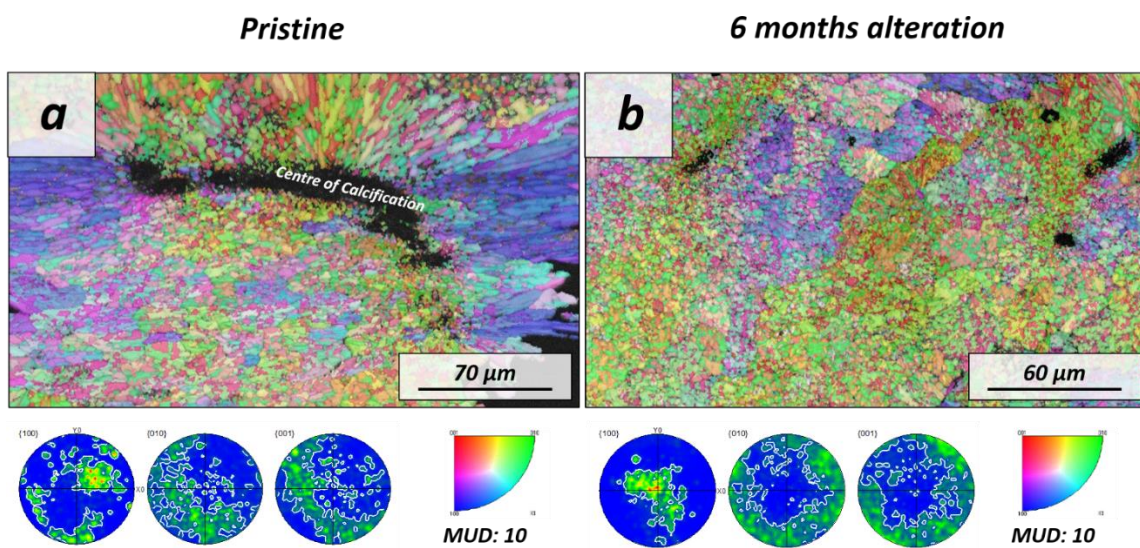


265 **Figure 4.** Vertical deflection AFM images depicting: (a-d) the pristine and (e-h) altered shells of the gastropod *Haliotis ovina*. The pristine shell of *Haliotis ovina* is composed of two layers: A prismatic shell layer and a nacreous inner portion consisting of an assembly of nacre tablets, formed by small rounded aragonitic subunits. (e-h) Upon hydrothermal alteration, calcite crystals, with their characteristic rhombohedral shape, form in the former biogenic prismatic layer. In both layers, we observe an amalgamation of mineral units. In the nacreous layer, boundaries of individual nacre tablets become blurred (white arrow in h). Cal: calcite crystals.

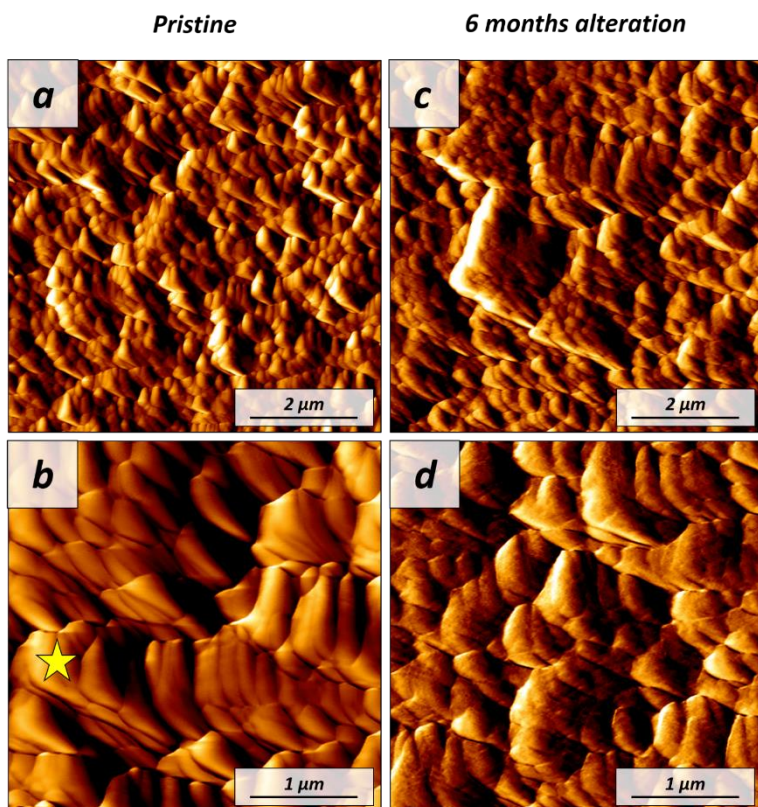


270 **Figure 5.** 3D surface reconstruction of height AFM measurements for aragonitic nacre tablets for: (a) pristine and (b) altered shell segments of the gastropod *Haliotis ovina*. In the pristine shell the organic membranes that separate adjacent tablets have a positive relief, while in the altered shell analogue a dramatic structural change is observable. At the site of the organic membrane we find a depression.

275 The modern skeleton of the scleractinian coral *Porites* sp. has a very compact microstructure in which spherulitic aragonitic units formed by acicular crystals grow radially around the calcification centres, the places where mineral nucleation starts (Fig. A11 and A12). EBSD data analyses show that acicular aragonite in *Porites* sp. has an average MUD value of 10 (Fig. 6 and A13). TGA analysis of the pristine *Porites* sp. skeletons show that the amount of organics in the sample is 2.1 wt. %. AFM images of the pristine skeleton of *Porites* sp. show that the aragonitic acicular crystals which build up this microstructure are
280 composed of aragonitic subunits of up to 1 µm (Fig. 7).



285 **Figure 6.** Colour-coded orientation maps with their corresponding pole figures derived from EBSD scans depicting the microstructure and texture of: (a) pristine and (b) altered coral, *Porites* sp., skeletons. Crystal co-orientation is given by the MUD value. No major changes can be observed between the pristine and the altered skeletal elements.



290 **Figure 7.** Vertical deflection AFM images of (a-b) pristine and (c-d) altered *Porites* sp. samples. The coral microstructure is formed by acicular aragonite crystals which, in turn, are composed of minute roundish subunits. Hydrothermal alteration experiments conducted in this study did not induce any significant change to the submicro to nanostructure of the coral skeleton.

295 3.2 The hydrothermally altered microstructures of *Arctica islandica*, *Haliotis ovina* and *Porites* sp. skeletons.

The interaction of the hard tissues of *Arctica islandica*, *Haliotis ovina* and *Porites* sp. with a burial mimicking fluid for up to 6 months at 80°C produces little to no transformation of the biogenic aragonite into abiogenic calcite, according to Rietveld analysis derived from XRD data (Fig. 8a, A2 and A14). Thus, after 6 months interaction with the burial fluid the total amount of calcite in the altered samples is approximately 16 wt. % in *Haliotis ovina*, 1 wt. % in *Arctica islandica* and less than 0.1 wt. % in *Porites* sp. It is remarkable that even though *Haliotis ovina* contains 16 wt. % of calcite after 6 months of alteration, this value is still only 0.8 wt. % after 4 months alteration.



TGA measurements show a reduction in the organic matter content of ~ 30 wt. % in *Arctica islandica* (from 2 wt. % to 1.3 wt. %), ~ 20 wt. % in *Haliotis ovina* (from 3.06 wt. % to 2.47 wt. %) and ~ 7 wt. % in *Porites* sp. (from 2.10 wt. % to 1.96 wt. %) (Fig. 8b and A3).

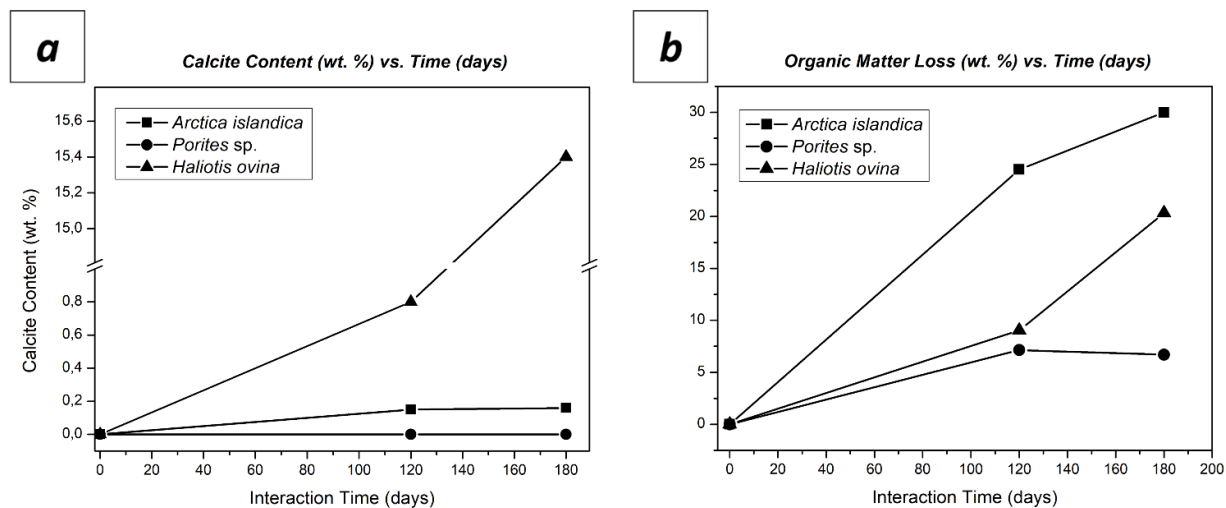


Figure 8. (a) Calcite content obtained from Rietveld analysis derived from XRD data and (b) organic matter loss measured with TGA with increasing alteration time. The influence of the individual aragonitic microstructure on both parameters is remarkable.

Laser confocal microscopy imaging was used to obtain overview images of sample surfaces to visualize main differences between the pristine and the altered samples (Fig. A4, A7 and A11). In the case of *Haliotis ovina*, new calcite crystals can be observed at the interphase between the aragonite prisms and the aragonite nacre tablets.

The microstructural evolution of the altered samples was followed with FE-SEM and EBSD measurements and the submicro- to nanostructural evolution of the altered samples was followed with AFM imaging. FE-SEM images of *Arctica islandica* shells altered for 6 months show no major changes compared to the pristine samples (Fig. A5). Contrarily, EBSD measurements show a big drop in the MUD value for the aragonite crystals which compose the shell of *Arctica islandica*. Thus, after 6 months interaction with the burial fluid, the MUD value of the outer layer of *Arctica islandica* shells drops from 8 to 4 while the MUD value of the crossed lamellar aragonite along the inner layer drops from 59 to 16, respectively (Fig. 1). AFM images taken in the altered shell of *Arctica islandica* show that crystal amalgamation occurs in the aragonite subunits of both shell layers (white arrows in Fig. 2).



325 In *Haliotis ovina*, FE-SEM images show large calcite crystals growing at the transition from nacreous to prismatic aragonite
(Fig. A8). The calcite crystals have a flat surface and are devoid of pores. Aragonite nacre tablets are subject to crystal/tablet
amalgamation, well observable as the boundaries between the different tablets become increasingly blurred with elapsing
interaction time (Fig. A8). FE-SEM, laser confocal microscopy imaging and EBSD measurements show that the large calcite
330 appear very bright in the band contrast map (Fig. A10) and show individual MUD values above 600, a MUD value close to
that of single calcite crystals precipitated from solution (Nindiyasari et al., 2014a; 2014b). The remaining, not transformed,
aragonite prisms undergo a significant drop in their MUD value from 19 in the pristine shell to 8 in the sample altered for 6
months. The amalgamation of the aragonite nacre tablets occurs concomitantly to a rapid increase in the MUD value of this
microstructure, which rockets from 91 in the pristine shell to 220 in the altered one. AFM images taken on the altered shells
335 of *Haliotis ovina* show new abiogenic calcite crystals growing within the aragonite prisms (Fig. 4). These calcite crystals have
a much smoother surface than the surface of the biogenic minerals in this work. The newly formed calcite crystals have straight
edges and, in some cases, allow us to see the characteristic rhombohedral morphology of the abiogenic calcite. The formation
of abiogenic calcite takes place concomitantly to an amalgamation of the aragonitic prisms similar to that observed in the
altered shells of *Arctica islandica* (white arrow in Fig. 4f). In the case of the aragonitic nacre tablets, it can be observed that in
340 this microstructure there is also amalgamation of the aragonite crystallites. Furthermore, the 3D topographic model of the
nacreous microstructure calculated from AFM height measurements shows that alteration produces an inversion in the
topography of the nacreous layer. Hence, the organic membranes between the nacre tablets, topographically elevated and well
observable in the pristine shell become depressed in the altered one. (Fig. 5)

345 The microstructure of the stony coral *Porites* sp. shows little change upon hydrothermal alteration after 6 months interaction
with a burial fluid at 80 °C. Neither FE-SEM imaging nor EBSD measurements show major differences between the pristine
and the altered sample. Furthermore, the MUD value of EBSD scans made on *Porites* sp. does not change after 6 months
alteration. Alike, the comparison of AFM images between pristine and altered shells does not indicate a significant
reorganization of the micro- and the nanostructure.

350 Statistical evaluation of grain size gained from EBSD measurements allows us to quantitatively evaluate grain size distribution
in the pristine and altered samples. The area of grains was grouped into clusters of 0.15 μm^2 (0.10 μm^2 in the case of the
aragonite nacre tablets for *Haliotis ovina*). These clusters are ordered by their relative frequencies and are shown in Fig. 9.
This data analysis was carried out for all the microstructures investigated in this study.

355

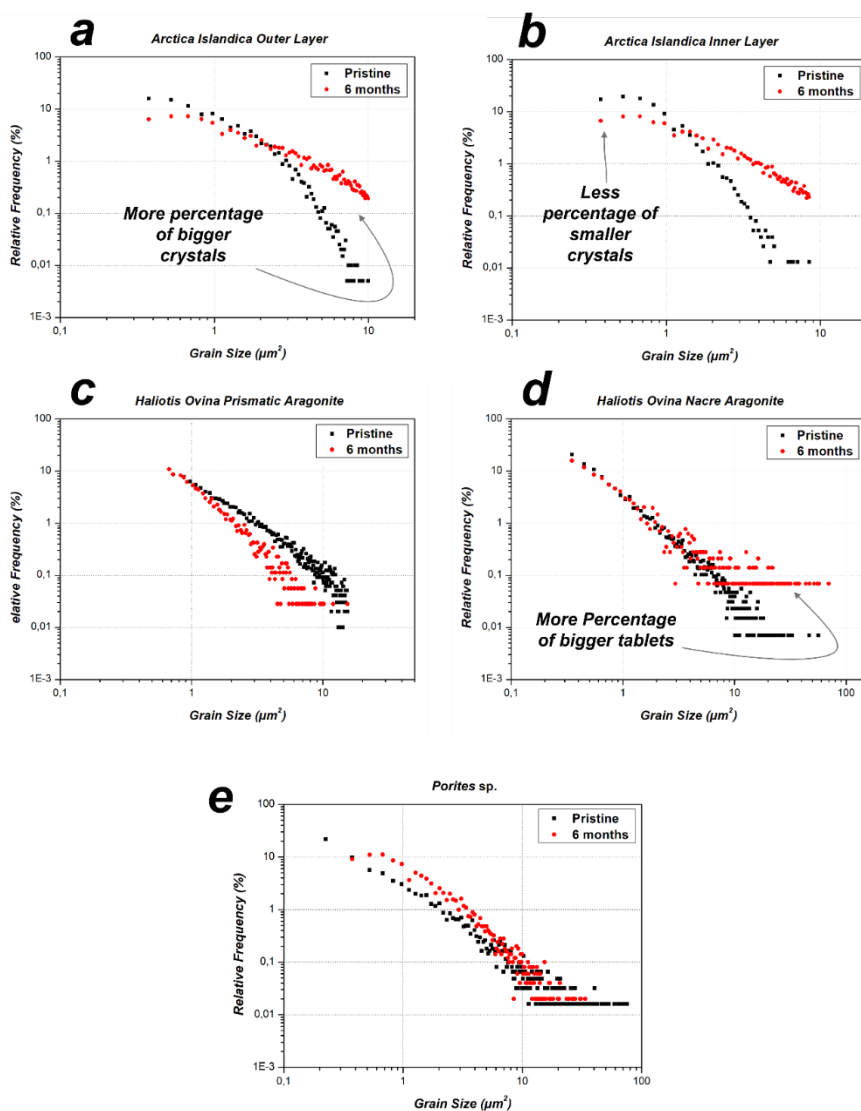


Figure 9. Relative frequency versus grain size/grain area for pristine and hydrothermally altered *Arctica islandica*, *Haliotis ovina* and *Porites* sp. shells and skeletal elements. (a, b): In *Arctica islandica* shells, there is a dramatic redistribution of grain size, such that the amount of smaller grains decreases, while the amount of larger grains in the shell increases. This occurs in both the outer and the inner layer of *Arctica islandica* shell. (c, d): In the shell of *Haliotis ovina*, the two layers follow a different evolution with progressive alteration. The grains in the prismatic layer decrease in size, while in the nacreous layer the amount of large grains increases. (e) For the coral *Porites* sp., we do not find significant variations in grain size/grain area with progressive alteration.



For the granular microstructure of *Arctica islandica* we see significant differences between the pristine and the altered shells. The observed differences are similar for both the outer and the inner layers of the animal. In the pristine shells of *Arctica islandica*, most of the grains have a small area. Thus, we find that 50.1% of the grains in the outer and 67.5% of the grains in the inner layer have an area smaller than $0.825 \mu\text{m}^2$. In contrast, only 0.91% of the grains of the outer layer and 0.13% of the grains of the inner layer have an area greater than $4.875 \mu\text{m}^2$. Interestingly, after 6 months hydrothermal alteration, a reduction in the number of small grains coupled to an increase in the number of large grains occurs (Table 1).

The two microstructures in *Haliotis ovina* shells also show a very different behaviour upon hydrothermal alteration. For aragonitic prisms, there is a general decrease in grain size. The distribution of the relative frequency of the clusters is similar in the pristine and in the altered sample. However, all the clusters of the altered sample are shifted to the left, that is, towards smaller grain sizes. In contrast, for nacre tablets most of the grain area data overlaps. An exception occurs with the largest tablets, whose frequency increases considerably between the pristine and the altered microstructures. Accordingly, the number of nacre tablets with an area greater than $5 \mu\text{m}^2$ increases from 5.1% in the pristine shell to 12.2% in the most altered one.

For *Porites* sp., we do not observe a major change of grain size/grain area between the pristine and the most altered sample. The majority of grain-area data overlaps.

Table 1. Change of aragonite grain area/grain size with increasing hydrothermal alteration for inner and outer layers of *Arctica islandica*. The drastic decrease in the number of smaller grains and the concomitant increase in the number of larger grains is striking.

		Grains smaller than $0.825 \mu\text{m}^2$	Grains bigger than $4.875 \mu\text{m}^2$
<i>Arctica Islandica</i> Outer Layer	Pristine Shell	50.1%	0.91%
	6 months altered shell	27.2%	23.1%
<i>Arctica Islandica</i> Inner Layer	Pristine Shell	67.5%	0.13%
	6 months altered shell	28.9%	18.7%

4 Discussion

4.1 The hydrothermal alteration of aragonitic hard tissues: A multi-step process

390

The effect of laboratory-based hydrothermal alteration of several aragonitic biominerals has recently been studied in great detail (Ritter et al., 2017; Casella 2017; Casella 2018; Pederson et al., 2019a, 2019b, 2020). A multi-analytical approach was



used to characterize the hard tissues, both pristine and after their alteration at temperatures above 100 °C with meteoric (Mg-free) and burial-mimicking (Mg-bearing) fluids. The comparison between aragonitic microstructures of the pristine and the altered samples reveals an alteration mechanism that consists of a sequence of intermediate and consecutive steps.

Structural materials secreted by organisms are composites of biopolymers and minerals arranged in hierarchical architectures (Weiner and Dove, 2003). In these composites mineral and organic matrices are intricately interrelated at all scale levels. This study, as well as previous ones, (Casella et al., 2018, Pederson et al., 2019a, 2019b, 2020) deciphered the main intermediate steps undergone by aragonitic microstructures during hydrothermal alteration. The alteration usually starts with the degradation of the biopolymers which are incorporated into the biocarbonate material. The fabric of the organic matter within the hard tissue is either a network of organic fibrils and/or a sequence of organic membranes. The degradation of the organic matter constitutes the first step of the hydrothermal alteration process and leads to the second alteration step, which consists in the formation of a network of pores that permeate the biomineral and facilitate the circulation of the hydrothermal fluid (Casella et al., 2017; Casella et al., 2018). As a result of this rather extensive phenomenon, local dissolution of bioaragonite occurs concomitantly to the precipitation of new, non-biogenic, aragonite (Casella et al., 2018). The precipitation of abiogenic aragonite is the third step of the hydrothermal alteration and results in an increase of aragonite grain size in the altered samples, relative to the size of the grains in their pristine counterparts (Casella et al., 2018). The fourth step of the hydrothermal alteration finally consists in the progressive replacement of both, biogenic as well as newly formed non-biogenic aragonite by new, non-biogenic calcite crystals (Casella et al., 2017; Casella et al., 2018). In this case, the extent of the replacement depends on a variety of factors, such as temperature, time, secondary porosity network features, fluid/solid ratio; and might be stopped before a complete replacement occurs (Sandberg and Hudson, 1983). Ritter et al., (2017) have also shown that the composition of the hydrothermal fluids can induce changes in the sequence of these alteration steps.

4.2 Hydrothermal alteration kinetics modulated by bioaragonite microstructures

Temperature and time are key parameters in defining the extent of the alteration of the aragonitic hard tissues when these are exposed to interaction with hydrothermal fluids (Ritter et al., 2017; Pederson et al., 2019a). Regardless of the specific microstructure of the biocarbonate material, longer interactions and higher temperatures lead to more extensive alterations and stronger overprints of the pristine features of the aragonitic skeletons. However, we observed that some characteristics of the pristine hard tissue make aragonitic biomaterials particularly resistant to hydrothermal alteration:

- (i) The primary porosity of the biomaterial defines the initial surface area of the microstructure that is exposed to the hydrothermal fluid and can react with it. Primary porosity strongly influences the very early stages of the alteration process (Casella et al., 2018; Greiner et al., 2018).



- 430 (ii) The amount, fabric, distribution and composition of the organic matter within the hard tissue define the characteristics of the secondary porosity network that results from biopolymer degradation during the first step of the hydrothermal alteration process. This secondary porosity network adds to the primary one and provides new pathways for the infiltration and circulation of the hydrothermal fluid within the biomaterial (Jonas et al., 2017; Casella et al., 2018). The tortuosity and permeability of this network, which depends on the shape, size and interconnectivity of its constituting pores (Forjanes et al., 2020a) define the extent of hydrothermal fluid infiltration through the hard tissue (Casella et al., 2018).
- 435 (iii) Microstructures in biological hard tissues result from an intimate interlinkage between minerals and organic matter, at all scale levels. This interlinkage determines that the architecture of the mineral component can influence the kinetics of the degradation of the organics and, thereby, modulate the formation of the secondary porosity network. Mineral microarchitecture and biopolymer characteristics are taxon or even specie-specific (Carter and Clark, 1985). This explains that different biological aragonitic hard tissues show different
440 susceptibility to hydrothermal alteration such that, while exposed to identical hydrothermal alteration conditions, some undergo a complete overprint of their pristine features, while others remain virtually unaltered (this study and Casella et al., 2018).
- 445 (iv) The solubility of the bioaragonite depends on factors such as crystal morphology, composition and amount of occluded biopolymers. Biogenic aragonite can incorporate small amounts of Sr^{2+} , Ba^{2+} and other ionic impurities into the crystal lattice. The presence of these impurities stresses the aragonite crystal structure and the resulting effect is an increase of aragonite solubility (Lippmann 1977, 1980, 1991; Plummer and Busenberg, 1987; Astilleros et al., 2003; Prieto 2009). Alike, the occlusion of biopolymer fibrils within biogenic aragonite crystals causes anisotropic lattice distortions of their lattice (Pokroy et al., 2006). This results as well in an increased
450 solubility of biogenic aragonite, relative to that of the non-biogenic equivalent (Chave et al., 1982; Busenberg and Plummer, 1985).
- 455 (v) The third step that marks the progress of the alteration of aragonitic hard tissues involves the dissolution of biogenic aragonite and the precipitation of non-biogenic aragonite. Consequently, the fourth step is given by the dissolution of both aragonite types, biogenic and non-biogenic, and the concomitant precipitation of abiogenic calcite. Small differences in aragonite solubility influence the development of the dissolution-crystallization reactions and affect the kinetics of the entire alteration process and mechanism.



460 It should be noted that, in the presence of fluids, porosity networks have a transient nature (Putnis, 2015). The dissolution-
crystallization reactions that take place during the third and fourth steps of the hydrothermal alteration process are connected
to solubility and molar volume changes. When, as a result of these changes, a partial or total obliteration of the biological hard
tissue porosity network takes place in the course of the third alteration step, the fourth step of the alteration process cannot
progress; it is either hindered or even totally precluded (Putnis et al., 2005; Jonas et al., 2014; Putnis, 2015).

465

4.3 The Role of Temperature and Time in the Hydrothermal Alteration of Aragonitic Hard Tissues.

Fig. 10 summarizes the different steps of the hydrothermal alteration process experienced by the outer and inner granular shell
layers of the bivalve *Arctica islandica*, the outer prismatic and inner nacreous layers of the shell of the gastropod *Haliotis*
470 *ovina* and the acicular, spherulitic, skeleton of the coral *Porites* sp. when being exposed to a burial fluid at (i) 175°C for 35
days (Casella et al., 2018; high-temperature/short-term alteration) and at (ii) 80°C for 6 months (this study; low-
temperature/long-term alteration). It is quite evident that, at both temperatures, the different hard tissues reach different stages
of hydrothermal alteration.

475 4.3.1 High Temperature – Short Term Experiments (Work of Casella et al., 2018)

At 175°C, the shell of *Arctica islandica* undergoes severe overprint with complete, in the outer layer, to extensive, in the inner
layer, replacement of the biogenic aragonite by abiogenic calcite. Significant overprint also affects the prismatic shell layer of
Haliotis ovina, which is extensively replaced by calcite. In contrast, the microstructures of the skeleton of *Porites* sp. and the
480 nacreous layer of *Haliotis ovina* shells are very resistant to hydrothermal overprint. Despite being resistant to alteration,
Haliotis ovina and *Porites* sp. show extensive formation of abiogenic aragonite. This leads to the amalgamation of aragonite
acicles and fibrils, in the *Porites* sp. skeleton, and of aragonite tablets, in the nacreous portion of the *Haliotis ovina* shell.
Nonetheless, the amount of biogenic aragonite replaced by abiogenic calcite is little in *Porites* sp. and negligible in *Haliotis*
ovina nacre tablets. The variability of the alteration kinetics of the above mentioned hard tissues at 175 °C was interpreted by
485 Casella et al., (2018) as arising from the combined effect of (i) the topological characteristics of the porosity network formed
as a consequence of biopolymer degradation (the first two steps of the alteration process) and (ii) the changes of the
microstructure of the biomaterial triggered by the porosity during the precipitation of new, abiogenic, aragonite (the third step
of the alteration process).

490 At temperatures above 160 °C, and in the presence of a hydrothermal fluid, biopolymers degrade rapidly, often within few
days (Benezeth et al., 1997; Jonas et al., 2017). In the outer and inner shell layers of *Arctica islandica* and in the prismatic
layer of the *Haliotis ovina* shell, aragonitic mineral units are immersed into a network of biopolymer fibrils (Casella et al.,
2018). The degradation of these fibrils results in a porosity network that is pervasive, consisting of large, interconnected pores,



and provides a pathway for the infiltration of the hydrothermal fluid. However, pore space is significantly reduced as new
495 aragonite precipitates during the third step of the hydrothermal alteration process (Ritter et al., 2017; Casella et al., 2018;
Pederson et al., 2019a, 2019b, 2020). The topological characteristics of this porosity network affect the replacement of the
aragonitic biological hard tissue by new, abiogenic, calcite, as increased aragonite surface becomes exposed to the
hydrothermal fluid. This leads to the significant overprint of the pristine features of granular *Arctica islandica* and prismatic
aragonite in *Haliotis ovina* hard tissues.

500

The behaviour of *Porites* sp. acicular and *Haliotis ovina* nacreous aragonite against hydrothermal alteration is different. The
skeleton of the coral *Porites* sp. has a vast primary porosity (Griesshaber et al., 2017; Casella et al., 2018). However, the
microstructure of this biological hard tissue is very dense and compact. Accordingly, little porosity is generated within the
bioaragonite as a result of biopolymer degradation. In addition, the scarce newly formed porosity disappears as aragonite fibres
505 abut with each other during the third step of hydrothermal alteration process (Casella et al., 2018). This reduces the surface
area of the bioaragonite that is in contact with the hydrothermal fluid. In the nacreous shell layer of *Haliotis ovina* the
degradation of organic sheaths around aragonite tablets generates a large porosity network. This porosity disappears during
the third hydrothermal alteration step due to abiogenic aragonite precipitation between the tablets and at the sites formerly
occupied by the organics. The resulting effect is extensive tablet amalgamation. Thus, in *Porites* sp. and *Haliotis ovina* nacre
510 tablets, abiogenic aragonite formation prevents the alteration to progress further and limits the overprint of the pristine features
of the hard tissue.

The Arrhenius equation predicts double reaction rate constants as temperature increases by 10°C (Arrhenius, 1889).
Accordingly, the temperature-dependent alteration processes should progress 20 times slower at 80°C than at 175°C. The more
515 sluggish kinetics of the alteration process explains that, despite the longer duration (180 days) of the experiments conducted
at 80°C, all investigated hard tissues undergo a much milder overprinting of their pristine features, relative to what is observed
in short-time experiments conducted at higher temperatures (e.g. Pederson et al., 2019a: (*Porites* sp. at 130°C altered for 8
weeks and at 160°C altered for 4 weeks; Jonas et al., 2017: *Porites* sp. and *Arctica islandica* altered at 200°C between 1 and
20 days).

520

Biopolymer degradation, which defines the first step of the hydrothermal alteration process and generates the secondary
porosity network, is, indeed, a temperature-dependent process (Moussout et al., 2016). Biopolymers decompose through
processes that involve depolymerization, bond scission, loss of functional groups and formation of free radicals (Gaffey 1988;
Gaffey et al., 1991). Under dry conditions, these processes take place very slowly up to temperatures that depend on the
525 composition and the structure of the biopolymer. Biopolymer decomposition temperatures can be as high as 250°C for small
biomolecules with simpler structures or might even be well above 300°C for larger and more complex biomolecules (Tiwari
and Raj, 2015). In the presence of water, biopolymer degradation accelerates significantly (Gaffey 1988; Gaffey et al., 1991;



530 Bénézeth et al., 1997) and can reach completion, when heated for 10^4 - 10^5 years, even at temperatures as low as 40°C - 80°C ;
the temperatures that prevail in the shallow burial diagenetic realm (Gaffey et al., 1991; Petrova et al., 2002; Le Bayon et al.,
2011).

The organic component of biological hard tissues consists of complex mixtures of polysaccharides, proteins, glycoproteins
and glycosaminoglycans and these degrade at different temperatures and rates (Gaffey, 1988; Gaffey et al., 1991; Tiwari and
Raj, 2015) and are specie-specific (Marie et al., 2011; Drake et al., 2013; Le Pabic et al., 2017). Accordingly, there will be
535 slightly different degradation pathways for the organic matter of the hard tissues of different organisms (Keenan and Engel,
2017). In addition, water-soluble and -insoluble macromolecules are found in the structural materials of biocarbonates (Weiner
and Traub, 1984; Goffredo et al., 2011; Sancho-Tomás et al., 2013). Therefore, it is likely that prior to complete degradation
of the biopolymer, the organic matrices will reorganize and some of their soluble components will be released into the alteration
fluid, especially at low temperatures. Since biopolymers contain a variety of functional groups, this release can influence the
540 progress of the hydrothermal alteration. It is well known that active moieties like peptide or carboxylic groups affect both the
dissolution and the crystallization of calcium carbonate polymorphs through a variety of mechanisms. This influence is
especially important when, as it occurs in the experiments conducted in this study, the fluid phase contains Mg^{2+} ions, as the
latter inhibit the crystallization of calcite and promote the formation of the less stable aragonite (Berner 1975; Fernández-Díaz
et al., 1996; Morse et al., 2007, De Choudens-Sanchez and González, 2009; Astilleros et al., 2010; Nielsen et al., 2013; Sun et
545 al., 2015). It has been reported that the inhibitory effect of Mg^{2+} ions for calcite crystallization can be overcome with
hydrophilic peptides since they enhance Mg^{2+} desolvation and shift the CaCO_3 polymorphic distribution towards the formation
of Mg-calcite (Stephenson et al., 2008; Wang et al., 2009; Nindiyasari et al., 2014a; 2014b; Yin et al., 2019). Similar Mg-
calcite crystallization-promoting effects have been observed in CaCO_3 crystallization experiments conducted in the presence
of proteinaceous extracts from a variety of coral skeletons (Sancho-Tomás et al., 2013, 2016).

550



Reaction Pathways during the Diagenesis of Aragonitic Biocarbonates

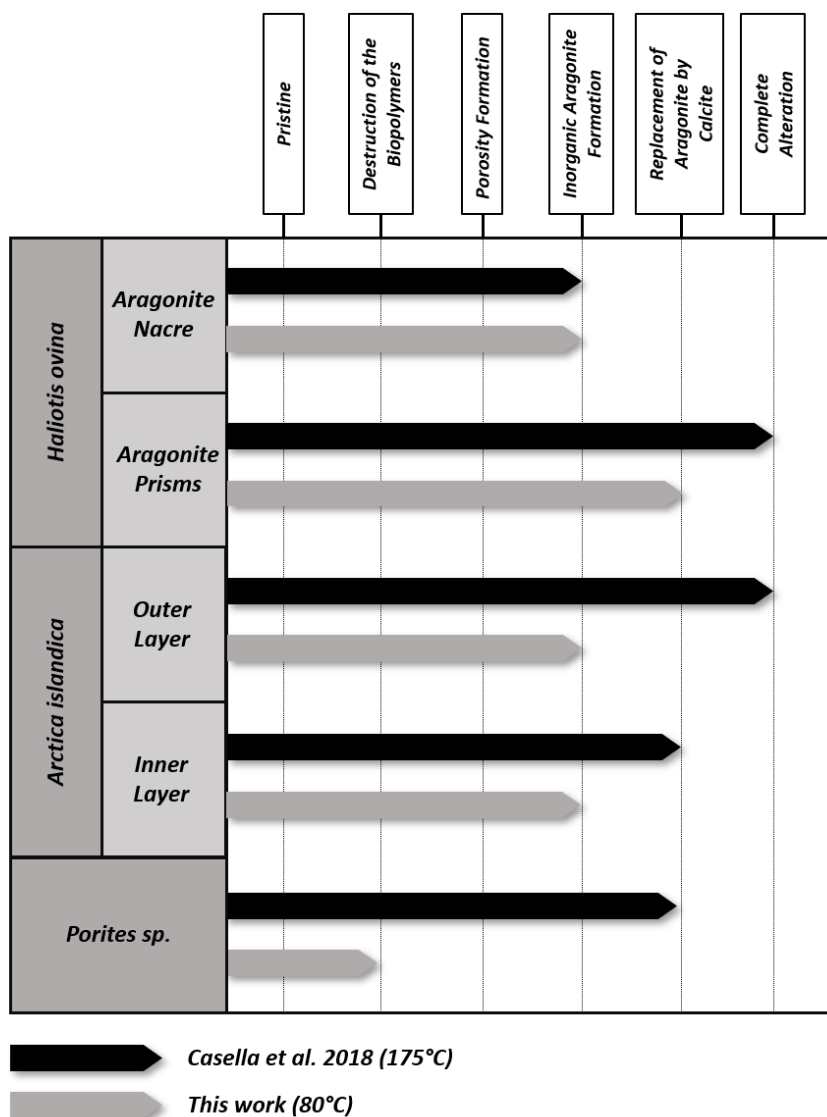


Figure 10. Main intermediate stages of alteration reached by the different aragonitic microstructures from this work when hydrothermally altered at 80°C (this work) and 175°C (Casella et al., 2018). In general, alteration at higher temperatures alter the microstructures more, so they reach further alteration stages. Contrarily, when the temperature is lower, the alteration is milder and the aragonitic microstructures reach previous alteration stages.



4.3.2 Long Temperature, Long Term Experiments (this work)

560

The organic matrix of *Porites* sp. and *Arctica islandica* is fully decomposed only at temperatures $\geq 160^{\circ}\text{C}$, while at 100°C only some dissolution and redistribution of the organics is observed even after 20 weeks of alteration (Jonas et al., 2017, Ritter et al., 2017; Pederson et al., 2019a, 2019b, 2020). In this work, though altered for even a longer time, 24 weeks, the slower kinetics of biopolymer decomposition at 80°C explains the small loss of organics in the case of *Porites* sp. Despite the high primary porosity of coral skeletons and the high amount of soluble macromolecules in coral organic matter, the smallest biopolymer loss (7 wt.%) is observed for the skeleton of *Porites* sp. This minor loss of organics is most likely a consequence of the combined effect of slow degradation kinetics coupled to the protecting effect of the very dense coral microstructure. The compactness of *Porites* sp. skeletal aragonite restricts the interaction between the organic substance and the hydrothermal fluid to the outer surfaces of the skeleton and to the calcification centres. Hence, significant biopolymer dissolution and remobilization within coral aragonite is hindered.

570

In contrast, significant decomposition of organic substance is found in the altered shells of *Haliotis ovina*. (20 wt.%) and *Arctica islandica*. (30 wt.%), respectively. This high impact of the low temperature hydrothermal conditions on the dissolution/decomposition of the organic substance is most likely a consequence of the less compact nature of the microstructures of these shells (Casella et al., 2018; Greiner et al., 2018), further modulated by the ratio between soluble and insoluble macromolecules and spatial arrangements of the organic matrix in *Haliotis ovina* and *Arctica islandica* hard tissues.

575

Our study shows that the difference in dissolution/decomposition of organics present within the hard tissues is a key parameter in the generation of different volumes of secondary porosity, which adds to the primary one initially present in the studied biomaterials. Accordingly, the hard tissue of *Porites* sp. shows a negligible 0.1 wt.% replacement of pristine bioaragonite by abiogenic calcite at 80°C . Pristine and altered samples of *Porites* sp. consist of aragonite crystals that are poorly co-oriented: EBSD scans show identical MUD values: 10 (Fig. 6). In addition, significant differences between the surfaces of pristine and altered *Porites* sp. samples cannot be detected. AFM images show that pristine and altered *Porites* sp. surfaces consist of similarly shaped and sized grains, without any detectable signs of mineral unit amalgamation. Statistical analysis of grain size distribution reports no significant difference in grain size between pristine and altered of *Porites* sp. samples. On the basis of all these findings we come to the conclusion that *Porites* sp. skeletons are extremely resistant to long-term hydrothermal alteration at low temperatures. This finding is in good agreement with the limited overprint experienced by *Porites* sp. skeletons in short-term hydrothermal alteration experiments, performed at significantly higher temperatures, 175°C (Casella et al., 2018; Pederson et al., 2019a).

585
590

The altered shell of *Arctica islandica* also exhibits at 80°C little replacement (1%wt) of aragonite by abiogenic calcite though, in this case, many of the original features of *Arctica islandica* shells appear moderately overprinted in the altered samples.



Compared to pristine *Arctica islandica* shells, altered samples consist of aragonite crystals that are less co-oriented, with a drop in the MUD values from 59 to 16 in the inner layer, and from 8 to 4 in the outer layer, respectively. The drop in aragonite
595 crystal co-orientation strength correlates with an increase in aragonite grain size. The growth in aragonite grain size is well detectable with AFM imaging (Fig. 5), where signs of crystal amalgamation are clearly visible. These changes can be explained as the result of the generation of a relatively small amount of secondary porosity, most likely due to remobilization and dissolution of soluble macromolecules. These may be released to the fluid at incipient decomposition of insoluble biopolymers. The poorly structured nature of inner and outer layers of the *Arctica islandica* shell facilitates the connection between pores in
600 the secondary porosity network and facilitates, accordingly, the interaction with the alteration fluid.

When the hydrothermal overprint starts, the fluid is equilibrated with atmospheric CO₂ and contains no Ca²⁺. Therefore, it is undersaturated with respect to aragonite, a disequilibrium that triggers the dissolution of the carbonate hard tissue. It was explained above that biogenic aragonites are more soluble than their abiogenic counterparts due to the anisotropic distortion
605 caused by the occlusion of biopolymers into the aragonite structure. Therefore, once the hydrothermal fluid in the pores becomes equilibrated with the biogenic aragonite of *Arctica islandica*, it becomes supersaturated with respect to abiogenic aragonite and, more so, with respect to calcite. At this stage, the nucleation of both phases is possible in the pores (Ruiz-Agudo et al., 2014).

Two main factors might promote the formation of abiogenic aragonite instead of abiogenic calcite: (i) the presence of Mg²⁺
610 ions in the fluid, which inhibits the nucleation and growth of calcite (Berner 1975; Fernández-Díaz et al., 1996; Morse et al., 2007, Astilleros et al., 2010; Nielsen et al., 2013), and, therefore, promotes the precipitation of metastable aragonite and, (ii) The energy barrier associated with heterogeneous nucleation, which is reduced when the substrate and the overgrowth have the same nature (Van der Merwe 1978; Chernov, 1984; Forjanés et al., 2020b). Therefore, the epitactic growth of aragonite on
615 the pre-existing aragonite grains is favoured over calcite. In our study, the formation of aragonite nuclei explains the increase in the average size of aragonite grains in altered samples. Since aragonite grains in pristine *Arctica islandica* shells are little co-oriented, epitactic growth of abiogenic aragonite can also cause a reduction in MUD values of the altered samples. In addition, epitactic growth of abiogenic aragonite leads to amalgamation of aragonite crystals and destruction of porosity. Reduction of porosity and crystal amalgamation limits the percolation of the hydrothermal fluid within the hard tissue and
620 prevents that the fourth alteration step, the replacement of aragonite by calcite, reaches any significance in any layer of *Arctica islandica* shells, at least within the duration of experiments conducted in this study.

The size distribution of aragonite crystals is different between pristine and altered *Arctica islandica* shells. Large-sized crystals are more frequent while small-sized crystals are less frequent, in both, the inner and the outer layers of altered *Arctica islandica*
625 shells, relative to those measured in the pristine hard tissue. This difference in grain size distribution can be explained by the development of an Ostwald ripening process in which the preferential dissolution of the smallest, less stable, aragonite grains



and the simultaneous growth of the largest crystals reduces the surface free energy of the system and results in an increase of the average aragonite crystal size and a shift of crystal size distribution towards higher values (Baronnet, 1982; Kile et al., 2000; Noguera et al., 2006; Vetter et al., 2013). Ostwald ripening processes occur under low levels of supersaturation, as it is the case for the biogenic aragonite dissolution-abiogenic aragonite precipitation reaction (Baronnet, 1982).

The strongest replacement of aragonite by abiogenic calcite during hydrothermal alteration at 80°C is observed in the shell of *Haliotis ovina* (16 wt.%). However, this replacement occurs exclusively in the prismatic shell layer, while, for the experiments conducted in this study, no replacement is observable in the nacreous shell layer of *Haliotis ovina*. Other hydrothermal alteration characteristics are also developed differently in the two shell layers of *Haliotis ovina*. While aragonite crystals in the prismatic shell layer become smaller sized and less co-oriented, with a drop from 19 to 8 in MUD value, in the nacreous layer the size and the co-orientation strength of aragonite crystals increase significantly with progressive overprint. The very different response of *Haliotis ovina* prismatic and nacreous layers to hydrothermal alteration is a consequence of their different microstructures as well as content and distribution of biopolymers. Nacre is the aragonitic microstructure with the highest content of biopolymers (Fig. 5). AFM imaging of the altered nacreous shell layer depicts the formation of grooves between the nacre tablets. This is indicative of an extensive dissolution/decomposition of the organic sheaths that envelope the tablets and results in the generation of a large volume of interconnected secondary porosity. This porosity facilitates the infiltration of the nacreous layer by the hydrothermal fluid.

The decay of biopolymers also generates a certain volume of secondary porosity in the prismatic shell layer. The less structured microstructure of this layer might induce that this porosity has also a high interconnectivity, even if its volume is smaller, relative to that of the nacreous shell layer. In both layers, secondary porosity guarantees the interaction with the hydrothermal fluid over an enlarged surface of the mineralized tissue. During the first 4 months of hydrothermal alteration there is no significant replacement of aragonite by calcite (Fig. A2). Therefore, it can be assumed that once the hydrothermal fluid equilibrates locally with the biogenic aragonite in the pores and becomes supersaturated with respect to abiogenic aragonite, aragonite nucleation will take place. Aragonite nucleation triggers the dissolution of biogenic aragonite and the crystallization of abiogenic aragonite through the formation of a dissolution-crystallization crystallization loops. (Putnis, 2002, 2009; Ruiz-Agudo et al., 2014). The evolution in crystal size distribution in the prismatic and the nacreous layers in *Haliotis ovina* indicates that this feedback affects both shell layers in a different way. Whereas the crystal size of the prismatic aragonite decreases during progressive alteration; the opposite occurs in the nacreous layer, where crystal size increases. The difference in aragonite crystal size evolution can be explained if most biogenic aragonite dissolution takes place in the prismatic layer and most abiogenic aragonite growth occurs in the nacreous layer. This interpretation is supported by the clear signs of nacre tablet amalgamation that is observed in AFM images of the altered nacreous shell layer (Fig. 4 and 5). A preferential epitactic nucleation and subsequent growth of abiogenic aragonite on nacre tablets explains the large increase in aragonite co-orientation strength in the nacreous layer during hydrothermal alteration at 80°C. Several factors can favour abiogenic aragonite nucleation



on nacre tables rather than on the aragonite prisms. Not all crystal surfaces are equally stable and the fibre-shaped crystals in the prismatic layer may be more prone to dissolution, relative to nacre tablets. Differences in the amount of biopolymer fibrils occluded in each type of crystals may also affect their relative stability. The epitactic growth of abiogenic aragonite on nacre tablets and the subsequent tablet amalgamation eliminates all the secondary porosity, making it very resistant to further hydrothermal alteration. Once nacre tablets growth is no longer possible, abiogenic calcite eventually nucleates within the prismatic layer. This nucleation triggers the aragonite dissolution-calcite crystallization reaction, whose development, though limited for the timespan of the performed experiments in this study, may have contributed to further decrease the size of the aragonite crystals in the prismatic layer of altered *Haliotis ovina* shell.

670 5 Conclusions

The susceptibility of biocarbonates to resist diagenetic overprint is strongly influenced by several primary features, such as the carbonate phase involved, the microstructure of the mineral component or the distribution and fabric of the organic matter within the composite hard tissue, among others. Laboratory-based hydrothermal alteration experiments offer important insights into the fate of biocarbonate hard tissues when responding to diagenetic alteration. While previous studies investigated the effect of high-temperature and short-term hydrothermal alteration on the change of biocarbonate microstructures (Casella et al., 2017, Casella et al., 2018, Pederson et al., 2019a, 2019b, 2020), the emphasis of this study is placed on the influence of low-temperature and long-term hydrothermal overprint processes of biologically secreted aragonite microstructures.

680 We deduce from our study the following conclusions:

1. We identify several intermediate stages during the overprint of aragonitic hard tissues: (I) decomposition of biopolymers, (II) gain of secondary porosity, (III) dissolution of the biogenic aragonite and precipitation of abiogenic aragonite, (IV) replacement of the biogenic and abiogenic aragonite by abiogenic calcite.
2. Depending on the composition, fabric and pattern of distribution of the organic matter within the biological hard tissue, the hydrothermal alteration induces the formation of secondary porosity. The latter porosity adds to the primary one and facilitates the penetration of the hydrothermal fluid.
3. The porosity network greatly affects the kinetics of the alteration process, irrespective of the alteration temperature. The tortuosity and permeability of the porosity network defines the extent of infiltration and percolation of the alteration fluid into the hard tissue. This explains that different biological aragonitic hard tissues show different susceptibilities to hydrothermal alteration. For similar alteration conditions, some microstructures undergo significant to complete overprint of their pristine features, while others remain virtually unaffected.



695

4. For most aragonitic microstructures, except for *Porites* sp. incipient formation of abiogenic aragonite is observed at the very beginning of the overprint process. Biogenic aragonite dissolves and recrystallizes into abiogenic aragonite.

700

5. Precipitation of abiogenic aragonite always occurs prior to calcite precipitation. This is supported by the observation of several processes affecting the aragonitic microstructures which take place without a phase change. These processes are: the increase in the size of the aragonite crystals, the amalgamation of adjacent crystals and the decrease in crystal co-orientation strength for amalgamated crystals.

705

6. The latter findings have major implications for paleoenvironmental reconstruction based on proxy data gained from fossil archives. Our findings suggest that, during the diagenesis, most fossil carbonate hard tissues are probably overprinted, even if they do not show clear signs of carbonate phase change.

Author contributions. PF, EG, LFD and WWS designed the study. NL provided sample material. PF performed the experiments. PF, MG, MSR, SVV conducted the analyses and carried out the evaluation and merging of data. PF, EG, JMA, LFD and drafted the manuscript. All authors contributed to discussions and the final manuscript.

Competing interests. The authors declare that they have no conflict of interest.

Acknowledgements. This study was supported by the MINECO (Spain) under project CGL2016-77138-C2-1-P. PF acknowledges a FPU predoctoral contract (FPU17/01689) from the Spanish Ministry of Universities. We acknowledge the European Union's Horizon 2020 Research and Innovation Program (Grant Agreement 643084) and the German Research Council Program (GR 9/1234)

6 References

720

Arrhenius, S.: Über die Reaktionsgeschwindigkeit bei der Inversion von Rohrzucker durch Säuren. Z. Phys. Chem., 4, 226-248, 1889.

725

Astilleros, J.M., Pina, C.M., Fernández-Díaz, L. and Putnis, A.: Metastable phenomena on calcite {1014} surfaces growing from Sr^{2+} - Ca^{2+} - CO_3^{2-} aqueous solutions. Chem. Geol., 193, 93-107, 2003.

Astilleros, J.M., Fernández-Díaz, L. and Putnis, A.: The role of magnesium in the growth of calcite: An AFM study. Chem. Geol., 271, 52-58, 2010.



- 730 Baronnet A.: Ostwald ripening: The case of calcite and mica. *Estud. Geol.*, 38, 185–198, 1982
- Bénézeth, P., Palmer, D. A., and Wesolowski, D. J.: Dissociation quotients for citric acid in aqueous sodium chloride media to 150 C. *J. Solut. Chem.*, 26, 63-84, 1997.
- 735 Berner, R. A.: The role of magnesium in the crystal growth of calcite and aragonite from sea water, *Geochim. Cosmochim. Ac.*, 39, 489–504, 1975.
- Bischoff, J. L.: Kinetics of calcite nucleation: magnesium ion inhibition and ionic strength catalysis, *J. Geophys. Res.*, 73, 3315–3322, 1968.
- 740
- Bischoff, J. L.: Temperature controls on aragonite-calcite transformation in aqueous solution, *Am. Mineral.*, 54, 149–155, 1969.
- Bischoff, W. D., Mackenzie, F. T., and Bishop, F. C.: Stabilities of synthetic magnesian calcites in aqueous solution: Comparison with biogenic materials. *Geochim. Cosmochim. Ac.*, 51, 1413-1423, 1987.
- 745
- Bischoff, W. D., Bertram, M. A., Mackenzie, F. T., and Bishop, F. C.: Diagenetic stabilization pathways of magnesian calcites. *Carbonates Evaporites*, 8, 82-89, 1993.
- 750 Busenberg, E. and Plummer, L.N.: Kinetic and thermodynamic factors controlling the distribution of SO_4^{2-} and Na^+ in calcites and selected aragonites. *Geochim. Cosmochim. Ac.*, 49, 713-725. 1985.
- Brand, U.: Biogeochemistry of Late Palaeozoic North American brachiopods and secular variation of seawater composition. *Biogeochemistry*, 7, 159-193, 1989.
- 755
- Cardew, P.T. and Davey, R.J.: The kinetics of solvent-mediated phase transformations. *Proc. R. Soc. A.*, 398, 415-428, 1985.
- Carter, J. G., and Clark, G. R.: Classification and phylogenetic significance of molluscan shell microstructure. *Studies in Geology, Notes for a Short Course*, 13, 50-71, 1985.
- 760 Casella, L.A., Griesshaber, E., Yin, X., Ziegler, A., Mavromatis, V., Müller, D., Ritter, A.C., Hippler, D., Harper, E.M., Dietzel, M. and Immenhauser, A.: Experimental diagenesis: insights into aragonite to calcite transformation of *Arctica islandica* shells by hydrothermal treatment. *Biogeosciences*, 14, 1461-1492, 2017.



- Casella, L.A., He, S., Griesshaber, E., Fernández-Díaz, L., Greiner, M., Harper, E.M., Jackson, D.J., Ziegler, A., Mavromatis, V., Dietzel, M. and Eisenhauer, A.: Hydrothermal alteration of aragonitic biocarbonates: assessment of micro- and nanostructural dissolution–reprecipitation and constraints of diagenetic overprint from quantitative statistical grain-area analysis. *Biogeosciences*, 15, 7451-7484, 2018.
- Chave, K. E., Deffeyes, K. S., Weyl, P. K., Garrels, R. M., and Thompson, M. E.: Observations on the solubility of skeletal carbonates in aqueous solutions. *Science*, 137, 33-34, 1982.
- Chernov, A. A.: Nucleation and epitaxy. In *Modern Crystallography III*, 48-103, 1984.
- Cherns, L., Wheeley, J.R. and Wright, V.P.: Taphonomic bias in shelly faunas through time: early aragonitic dissolution and its implications for the fossil record. In *Taphonomy*, 79-105, 2011.
- Cherns, L. and Wright, V. P.: Skeletal mineralogy and biodiversity of marine invertebrates: size matters more than seawater chemistry. *Geological Society, London, Special Publications*, 358, 9-17, 2011.
- De Choudens-Sanchez, V. and Gonzalez, L.A.: Calcite and aragonite precipitation under controlled instantaneous supersaturation: elucidating the role of CaCO₃ saturation state and Mg/Ca ratio on calcium carbonate polymorphism. *J. Sediment. Res.*, 79, 363-376, 2009.
- Drake, J. L., Mass, T., Haramaty, L., Zelzion, E., Bhattacharya, D., and Falkowski, P. G.: Proteomic analysis of skeletal organic matrix from the stony coral *Stylophora pistillata*. *Proceedings of the National Academy of Sciences*, 110, 3788-3793, 2013.
- Fernandez-Diaz, L., Putnis, A., Prieto, M. and Putnis, C.V.: The role of magnesium in the crystallization of calcite and aragonite in a porous medium. *J. Sediment. Res.*, 66, 482-491, 1996.
- Forjanés, P., Astilleros, J. M., and Fernández-Díaz, L.: The formation of barite and celestite through the replacement of gypsum. *Minerals*, 10, 189, 2020a.
- Forjanés, P., Gómez-Barreiro, J., Morales, J., Astilleros, J. M., and Fernández-Díaz, L.: Epitactic growth of celestite on anhydrite: substrate induced twinning and morphological evolution of aggregates. *CrystEngComm*, 22, 5743-5759, 2020b.
- Fyfe, W. S. and Bischoff, J. L.: The calcite-aragonite problem, *Soc. Econ. Pa.*, 13, 3–13, 1965.



- Gaffey, S.J.: Water in skeletal carbonates. *J. Sediment. Res.* 58, 397–414, 1988.
- 800 Gaffey, S.J., Kolak, J.J., and Bronnimann, C.E.: Effects of drying, heating, annealing, and roasting on carbonate skeletal material, with geochemical and diagenetic implications. *Geochim. Cosmochim. Ac.*, 55, 1627–1640, 1991.
- Gebauer, D. and Cölfen, H.: Prenucleation clusters and nonclassical nucleation, *Nano Today*, 6, 564–584, 2011.
- 805 Gebauer, D., Völkel, A., and Cölfen, H.: Stable prenucleation calcium carbonate Clusters, *Science*, 322, 1819–1822, 2008.
- Goffredo, S., Vergni, P., Reggi, M., Caroselli, E., Sparla, F., Levy, O., Dubinsky, Z. and Falini, G.: The skeletal organic matrix from Mediterranean coral *Balanophyllia europaea* influences calcium carbonate precipitation. *PLoS One*, 6, 22338, 2011.
- 810 Greiner, M.; Fernández-Díaz, L.; Griesshaber, E.; Zenkert, M.N.; Yin, X.; Ziegler, A.; Veintemillas-Verdaguer, S.; Schmahl, W.W.: Biomineral Reactivity: The Kinetics of the Replacement Reaction of Biological Aragonite to Apatite. *Minerals*, 8, 315, 2018.
- Griesshaber, E., Schmahl, W. W., Ubhi, H. S., Huber, J., Nindiyasari, F., Maier, B., and Ziegler, A.: Homoepitaxial meso- and
815 microscale crystal co-orientation and organic matrix network structure in *Mytilus edulis* nacre and calcite. *Acta Biomater.*, 9, 9492-9502, 2013.
- Griesshaber, E., Yin, X., Ziegler, A., Kelm, K., Checa, A., Eisenhauer, A., and Schmahl, W. W.: Patterns of mineral organization in carbonate biological hard materials. In *Highlights in applied mineralogy*, 245-272, 2017.
- 820 Hall, A., Kennedy, W. J., and Taylor, J. H.: Aragonite in fossils. *Proc. R. Soc. Lond. B Biol. Sci.*, 168, 377-412, 1967.
- Hallam, A., and O'Hara, M.J.: Aragonitic fossils in the Lower Carboniferous of Scotland. *Nature*, 195, 273-274, 1962.
- 825 James, N. P., Bone, Y., and Kyser, T. K.: Where has all the aragonite gone? Mineralogy of Holocene neritic cool-water carbonates, southern Australia. *J. Sediment. Res.*, 75, 454-463, 2005.
- Janiszewska, K., Mazur, M., Machalski, M., and Stolarski, J.: From pristine aragonite to blocky calcite: Exceptional preservation and diagenesis of cephalopod nacre in porous Cretaceous limestones, *Plos one*, 13, e0208598, 2018.



- 830 Jarosch, D., and Heger, G.: Neutron diffraction refinement of the crystal structure of aragonite. *Tscher. Mineral. Petr. Mitt.*, 35, 127-131, 1986.
- Jonas, L., John, T., King, H. E., Geisler, T., and Putnis, A.: The role of grain boundaries and transient porosity in rocks as fluid pathways for reaction front propagation. *Earth Planet. Sci. Lett.*, 386, 64-74, 2014.
- 835 Jonas, L., Müller, T., Dohmen, R., Immenhauser, A., and Putlitz B.: Hydrothermal replacement of biogenic and abiogenic aragonite by Mg-carbonates—Relation between textural control on effective element fluxes and resulting carbonate phase. *Geochim. Cosmochim. Ac.*, 196, 289-306, 2017.
- 840 Keenan, S. W., and Engel, A. S.: Early diagenesis and recrystallization of bone. *Geochim. Cosmochim. Ac.*, 196, 209-223, 2017.
- Kile, D. E., Eberl, D. D., Hoch, A. R., and Reddy, M. M.: An assessment of calcite crystal growth mechanisms based on crystal size distributions. *Geochim. Cosmochim. Ac.*, 64, 2937-2950, 2000.
- 845 Le Bayon, R., Brey, G. P., Ernst, W. G., and Mählmann, R. F.: Experimental kinetic study of organic matter maturation: Time and pressure effects on vitrinite reflectance at 400 C. *Org. Geochem.*, 42, 340-355, 2011.
- Le Pabic, C., Marie, A., Marie, B., Percot, A., Bonnaud-Ponticelli, L., Lopez, P. J., and Luquet, G.: First proteomic analyses of the dorsal and ventral parts of the *Sepia officinalis* cuttlebone. *J. Proteom.*, 150, 63-73, 2017.
- 850 Lippmann F.: The solubility product of complex minerals, mixed crystals and three-layer clay minerals. *N. Jahrb. Mineral. Abh.*, 130, 243-263, 1977.
- Lippmann F.: Phase diagrams depicting the aqueous solubility of binary mineral systems. *N. Jahrb. Mineral. Abh.*, 139, 1-25, 855 1980.
- Lippmann F.: Aqueous solubility of magnesian calcites with different endmembers. *Acta. Mineral. Petrogr.*, 32, 5-19. 1991.
- Lowenstam, H.A.: Factors affecting the aragonite: calcite ratios in carbonate-secreting marine organisms. *J. Geol.*, 62, 284- 860 322, 1954.
- Marie, B., Le Roy, N., Zanella-Cléon, I., Becchi, M., and Marin, F.: Molecular evolution of mollusc shell proteins: insights from proteomic analysis of the edible mussel *Mytilus*. *J. Mol. Evol.*, 72, 531-546, 2011.



- 865 Markgraf, S. A., and Reeder, R. J.: High-temperature structure refinements of calcite and magnesite. *Am. Min.*, 70, 590-600, 1985.
- Morse, J. W., Arvidson, R. S., and Lüttge, A.: Calcium carbonate formation and dissolution, *Chem. Rev.*, 107, 342–381, 2007.
- 870 Moussout, H., Ahlafi, H., Aazza, M., and Bourakhouadar, M.: Kinetics and mechanism of the thermal degradation of biopolymers chitin and chitosan using thermogravimetric analysis. *Polymer Degradation and Stability*, 130, 1-9, 2016.
- Mucci, A., Canuel, R., and Zhong, S.: The solubility of calcite and aragonite in sulfate-free seawater and the seeded growth kinetics and composition of the precipitates at 25 C. *Chem. Geol.*, 74, 309-320, 1989.
- 875
- Navrotsky, A.: Energetic clues to pathways to biomineralization: Precursors, clusters, and nanoparticles, *P. Natl. Acad. Sci. USA.*, 101, 12096–12101, 2004.
- Nielsen, L. C., De Yoreo, J. J., and DePaolo, D. J.: General model for calcite growth kinetics in the presence of impurity ions. *Geochim. Cosmochim. Ac.*, 115, 100-114, 2013.
- 880
- Nindiyasari, F., Fernández-Díaz, L., Griesshaber, E., Astilleros, J. M., Sanchez-Pastor, N., and Schmahl, W. W.: Influence of gelatin hydrogel porosity on the crystallization of CaCO₃, *Cryst. Growth Des.*, 14, 1531–1542, 2014a.
- 885 Nindiyasari, F., Griesshaber, E., Fernandez-Diaz, L., Astilleros, J. M., Sanchez-Pastor, N., Ziegler, A., and Schmahl, W. W.: Effects of Mg and hydrogel solid content on the crystallization of calcium carbonate in biomimetic counter-diffusion systems. *Cryst. Growth Des.*, 14, 4790-4802, 2014b.
- Noguera, C., Fritz, B., Clément, A., and Baronnet, A.: Nucleation, growth, and ageing scenarios in closed systems I: A unified mathematical framework for precipitation, condensation and crystallization. *J. Cryst. Growth.*, 297, 180-186, 2006.
- 890
- Pederson, C.L., Weiss, L., Mavromatis, V., Rollion-Bard, C., Dietzel, M., Neuser, R. and Immenhauser, A.: Significance of fluid chemistry throughout diagenesis of aragonitic *Porites* corals—An experimental approach. *Depos. Rec.*, 5, 592-612, 2019a.
- 895 Pederson, C., Mavromatis, V., Dietzel, M., Rollion-Bard, C., Nehrke, G., Jöns, N., Jochum, K.P. and Immenhauser, A.: Diagenesis of mollusc aragonite and the role of fluid reservoirs. *Earth Planet. Sci. Lett.*, 514, 130-142, 2019b.



- 900 Pederson, C.L., Mavromatis, V., Dietzel, M., Rollion-Bard, C., Breitenbach, S.F.M., Yu, D., Nehrke, G. and Immenhauser, A.: Variation in the diagenetic response of aragonite archives to hydrothermal alteration. *Sediment. Geol.*, 406, 105716, 2020.
- Perdikouri, C., Kasioptas, A., Putnis, C.V. and Putnis, A.: The effect of fluid composition on the mechanism of the aragonite to calcite transition. *Mineral. Mag.*, 72, 111-114, 2008.
- Perdikouri, C., Kasioptas, A., Geisler, T., Schmidt, B. C., and Putnis, A.: Experimental study of the aragonite to calcite transition in aqueous solution, *Geochim. Cosmochim. Ac.*, 75, 6211–6224, 2011.
- 905 Perdikouri, C., Piazzolo, S., Kasioptas, A., Schmidt, B. C., and Putnis, A.: Hydrothermal replacement of Aragonite by Calcite: interplay between replacement, fracturing and growth, *Eur. J. Mineral.*, 25, 123–136, 2013.
- 910 Petrova, T. V., Mahlmann, R. F., Stern, W. B., and Frey, M.: Application of combustion and DTA-TGA analysis to the study of metamorphic organic matter. *Schweiz Mineral Petrogr Mitt.*, 82, 33-53, 2002.
- Plummer, L. N. and Mackenzie, F. T.: Predicting mineral solubility from rate data; application to the dissolution of magnesian calcites, *Am. J. Sci.*, 274, 61–83, 1974.
- 915 Plummer, L. N. and Busenberg, E.: The solubilities of calcite, aragonite and vaterite in CO₂-H₂O solutions between 0 and 90 °C, and an evaluation of the aqueous model for the system CaCO₃- CO₂-H₂O, *Geochim. Cosmochim. Ac.*, 46, 1011–1040, 1982.
- 920 Plummer, L. N., and Busenberg, E.: Thermodynamics of aragonite-strontianite solid solutions: Results from stoichiometric solubility at 25 and 76 C. *Geochim. Cosmochim. Ac.*, 51, 1393-1411, 1987.
- Pokroy, B., Fitch, A. N., Lee, P. L., Quintana, J. P., El'ad, N. C., and Zolotoyabko, E.: Anisotropic lattice distortions in the mollusk-made aragonite: a widespread phenomenon. *J. Struct. Biol.*, 153, 145-150, 2006.
- 925 Prieto, M.: Thermodynamics of solid solution-aqueous solution systems. *Rev. Mineral. Geochem.*, 70, 47-85, 2009.
- Putnis, A.: Mineral replacement reactions: from macroscopic observations to microscopic mechanisms. *Mineral. Mag.*, 66, 689-708, 2002.
- 930 Putnis, A.: Mineral replacement reactions. *Rev. Mineral. Geochem.*, 70, 87-124, 2009.



- Putnis, A.: Transient porosity resulting from fluid–mineral interaction and its consequences. *Rev. Mineral. Geochem.*, 80, 1-23, 2015.
- 935
- Putnis, C. V., Tsukamoto, K., and Nishimura, Y.: Direct observations of pseudomorphism: compositional and textural evolution at a fluid-solid interface. *Am. Min.*, 90, 1909-1912, 2005.
- Putnis, A. and Putnis, C.V.: The mechanism of reequilibration of solids in the presence of a fluid phase. *J. Solid State Chem.*, 940 180, 1783-1786, 2007.
- Radha, A. V. and Navrotsky, A.: Thermodynamics of carbonates, *Rev. Mineral. Geochem.*, 77, 73–121, 2013.
- Radha, A. V., Forbes, T. Z., Killian, C. E., Gilbert, P. U. P. A., and Navrotsky, A.: Transformation and crystallization energetic 945 of synthetic and biogenic amorphous calcium Carbonate, *PNAS*, 107, 16438–16443, 2010.
- Randle, V.: Theoretical framework for electron backscatter diffraction. In *Electron backscatter diffraction in materials science*, 19-30, 2000.
- 950 Redfern, S. A. T., Salje, E., and Navrotsky, A.: High-temperature enthalpy at the orientational order-disorder transition in calcite: implications for the calcite/aragonite phase equilibrium, *Contrib. Mineral. Petr.*, 101, 479–484, 1989.
- Ritter, A.C., Mavromatis, V., Dietzel, M., Kwiecien, O., Wiethoff, F., Griesshaber, E., Casella, L.A., Schmahl, W.W., Koelen, J., Neuser, R.D. and Leis, A.: Exploring the impact of diagenesis on (isotope) geochemical and microstructural alteration 955 features in biogenic aragonite. *Sedimentology*, 64, 1354-1380, 2017.
- Rodríguez-Carvajal, J.: FullProf. CEA/Saclay, France, 2001.
- Ruiz-Agudo, E., Putnis, C.V. and Putnis, A.: Coupled dissolution and precipitation at mineral–fluid interfaces. *Chem. Geol.*, 960 383, 132-146, 2014.
- Sancho-Tomás, M., Fermani, S., Durán-Olivencia, M. A., Otálora, F., Gómez-Morales, J., Falini, G., and García-Ruiz, J. M.: Influence of charged polypeptides on nucleation and growth of CaCO₃ evaluated by counterdiffusion experiments. *Cryst. Growth Des.*, 13, 3884-3891, 2013.



- Sancho-Tomás, M., Fermani, S., Reggi, M., García-Ruiz, J. M., Gómez-Morales, J., and Falini, G.: Polypeptide effect on Mg^{2+} hydration inferred from $CaCO_3$ formation: a biomineralization study by counter-diffusion. *CrystEngComm*, 18, 3265-3272, 2016.
- 970 Sandberg, P.A. and Hudson, J.D.: Aragonite relic preservation in Jurassic calcite-replaced bivalves. *Sedimentology*, 30, 879-892, 1983.
- Sass, E., Morse, J. W., and Millero, F. J.: Dependence of the values of calcite and aragonite thermodynamic solubility products on ionic models, *Am. J. Sci.*, 283, 218–229, 1983.
- 975 Schmidt, N. H., and Olesen, N. O.: Computer-aided determination of crystal-lattice orientation from electron channeling patterns in the SEM. *Canad. Mineral.*, 27, 15-22, 1989.
- Seuß, B., Nützel, A., Mapes, R. H., and Yancey, T. E.: Facies and fauna of the Pennsylvanian Buckhorn Asphalt Quarry deposit: a review and new data on an important Palaeozoic fossil Lagerstätte with aragonite preservation. *Facies*, 55, 609, 2009.
- 980 Stephenson, A. E., DeYoreo, J. J., Wu, L., Wu, K. J., Hoyer, J., and Dove, P. M.: Peptides enhance magnesium signature in calcite: insights into origins of vital effects. *Science*, 322, 724-727, 2008.
- 985 Sun, W., Jayaramana, S., Chen, W., Persson, K. A., and Cedera, G.: Nucleation of metastable aragonite $CaCO_3$ in seawater, *PNAS*, 112, 3199–3204, 2015.
- Swart, P. K.: The geochemistry of carbonate diagenesis: The past, present and future. *Sedimentology*, 62, 1233-1304, 2015.
- 990 Tiwari A, and Raj B.: *Reactions and Mechanisms in Thermal Analysis of Advanced Materials*. New York: John Wiley and Sons, 2015.
- Van Der Merwe J.H.: The role of lattice misfit in epitaxy, *Crit. Rev. Solid. State. Mater. Sci.*, 7, 209–231, 1978
- 995 Vetter, T., Iggländ, M., Ochsenbein, D. R., Hänseler, F. S., and Mazzotti, M.: Modeling nucleation, growth, and Ostwald ripening in crystallization processes: a comparison between population balance and kinetic rate equation. *Cryst. Growth Des.*, 13, 4890-4905, 2013.



1000 Walter, L. M., and Morse, J. W.: Reactive surface area of skeletal carbonates during dissolution; effect of grain size. *J. Sediment. Res.*, 54, 1081-1090, 1984.

Wang, D., Wallace, A. F., De Yoreo, J. J., and Dove, P. M.: Carboxylated molecules regulate magnesium content of amorphous calcium carbonates during calcification. *Proc. Natl. Acad. Sci.*, 106, 21511-21516, 2009.

1005

Weiner, S., and Traub, W.: Macromolecules in mollusc shells and their functions in biomineralization. *Philos. Trans. R. Soc. B.*, 304, 425-434, 1984.

Weiner, S., and Dove, P. M.: An overview of biomineralization processes and the problem of the vital effect. *Rev. Mineral. Geochem.*, 54, 1-29, 2003.

1010

Wright, V. P. and Cherns, L.: Are there “black holes” in carbonate deposystems? *Geol. Acta*, 2, 285–290, 2004.

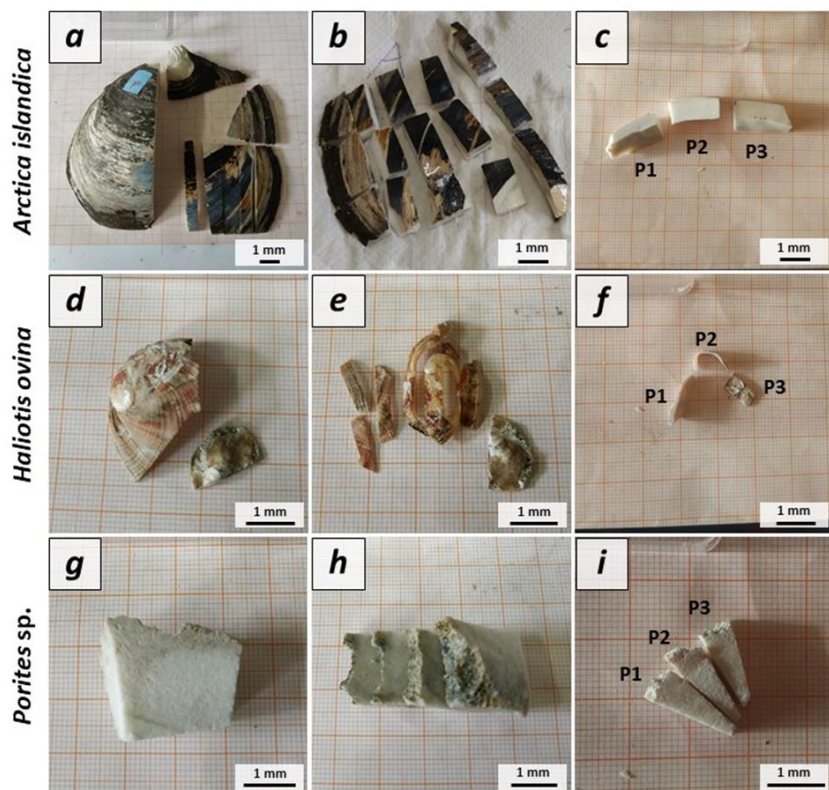
Wright, V. P., Cherns, L., and Hodges, P.: Missing molluscs: Field testing taphonomic loss in the Mesozoic through early large scale aragonite dissolution, *Geology*, 31, 211–214, 2003.

1015

Yin, X., Griesshaber, E., Fernandez-Diaz, L., Ziegler, A., García-García, F. J., and Schmahl, W. W.: Influence of Gelatin–Agarose Composites and Mg on Hydrogel-Carbonate Aggregate Formation and Architecture. *Cryst. Growth Des.*, 19, 5696-5715, 2019.

1020

Appendix Figures



1025 **Figure A1.** Preparation of *Arctica islandica*, *Haliotis ovina* shells and *Porites* sp. skeletons for hydrothermal alteration experiments. A long section was cut out of the hard tissue (Figs. A1a, d, g). Subsequently, it was sectioned into three parts: P1, P2, P3 (Figs. A1b, e, h). The pieces were then altered. P1 was used for laser confocal microscopy and atomic force microscopy (AFM) imaging; P2 was used for FE-SEM imaging and EBSD measurements and P3 was powdered and used for XRD and TGA measurements; the XRD data formed the basis for Rietveld refinements.

1030

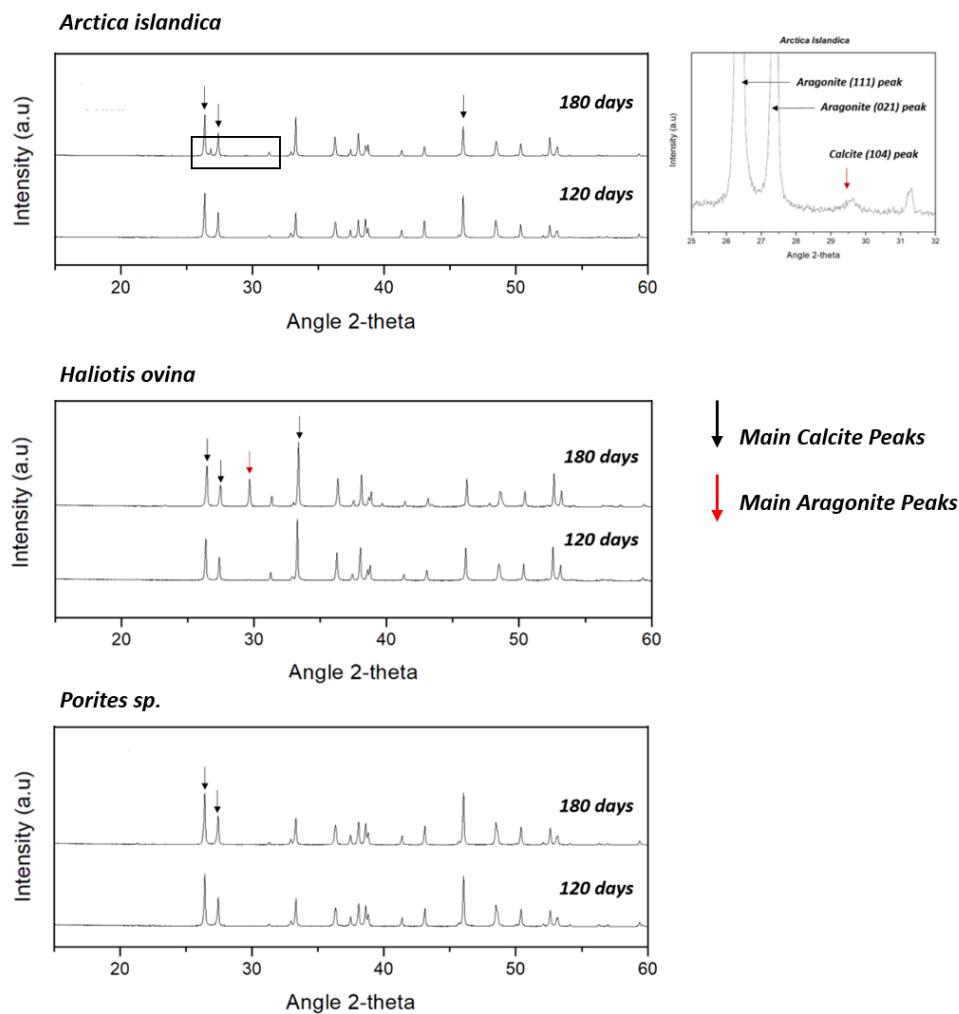


Figure A2. X-ray diffractograms of the hydrothermally altered shells and skeletons of *Arctica islandica*, *Haliotis ovina* and *Porites sp.* Alteration was performed at 80°C in a Mg-rich, burial, (100 mM NaCl + 10 mM MgCl₂) and lasted for 4 and 6 months.

1035

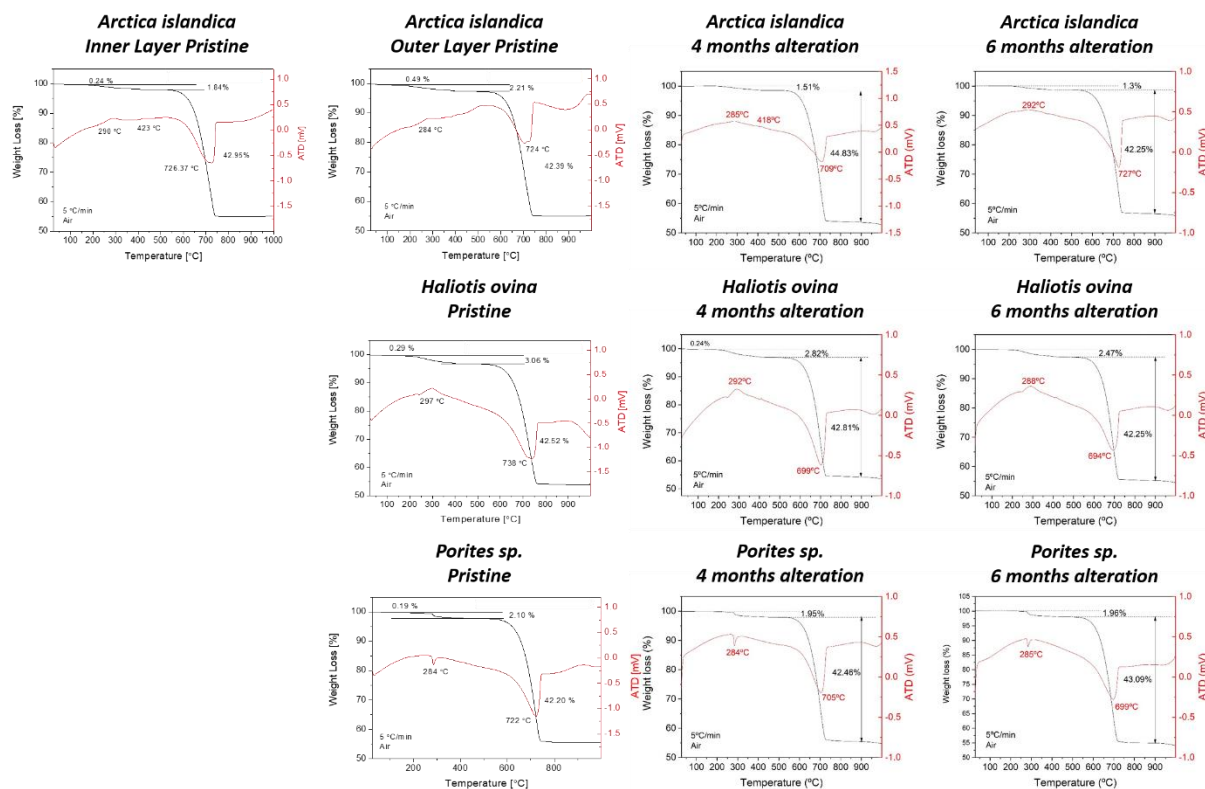


Figure A3. Thermogravimetric analysis data of pristine and altered hard tissues of *Arctica islandica*, *Haliotis ovina* and *Porites* sp. shells and skeletal elements. Alteration was performed at 80°C in a Mg-rich, burial, (100 mM NaCl + 10 mM MgCl₂) and lasted for 4 and 6 months.

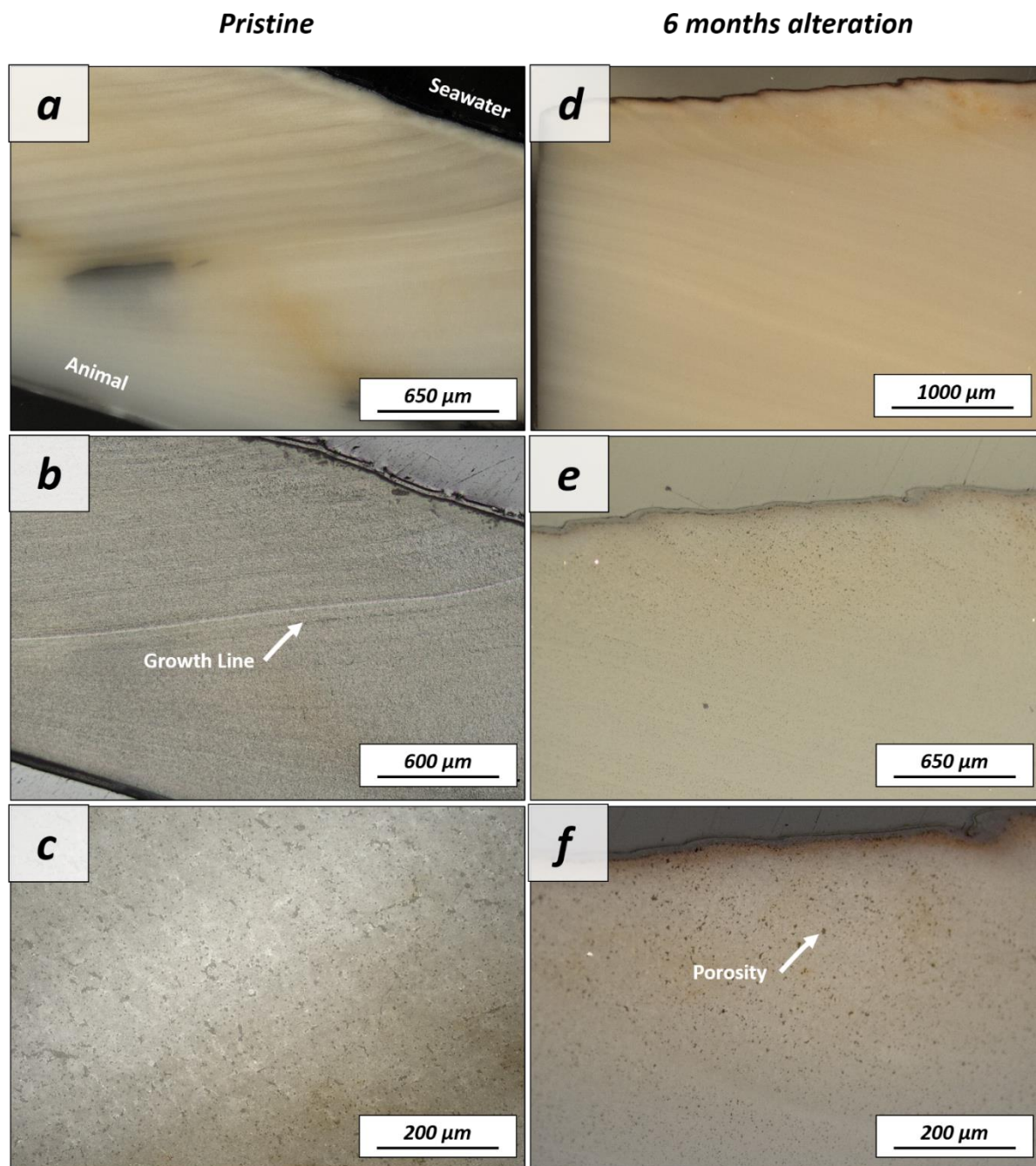
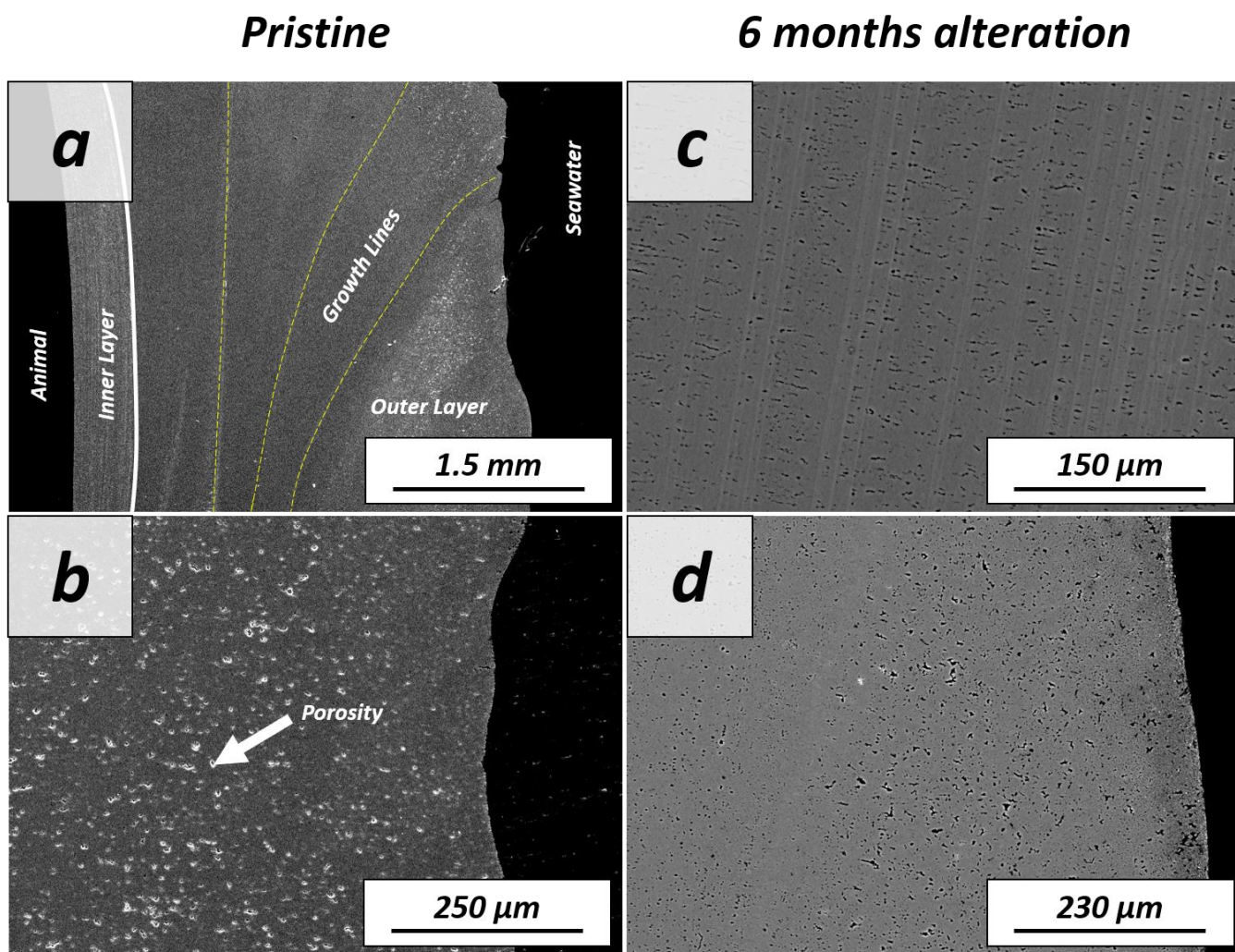


Figure A4. Laser confocal microscopy images of (a-c) pristine and (d-f) altered shells of *Arctica islandica*. The shells display a homogeneous internal structure where porosity and growth lines can be observed. After 6 months of hydrothermal alteration, major changes to the shell structure cannot be observed with laser confocal microscopy imaging.



1050

Figure A5. FE-SEM images of (a,b) pristine and (c,d) altered shells of the bivalve *Arctica islandica*. The shell consists of an assemblage of irregular aragonite crystals embedded in a network of biopolymer fibres (this study and Casella et al., 2017; 2018). Two layers comprise the shell, both with abundant pores and growth lines (c,d). Hydrothermal alteration at 80 °C in

1055 FE-SEM imaging.

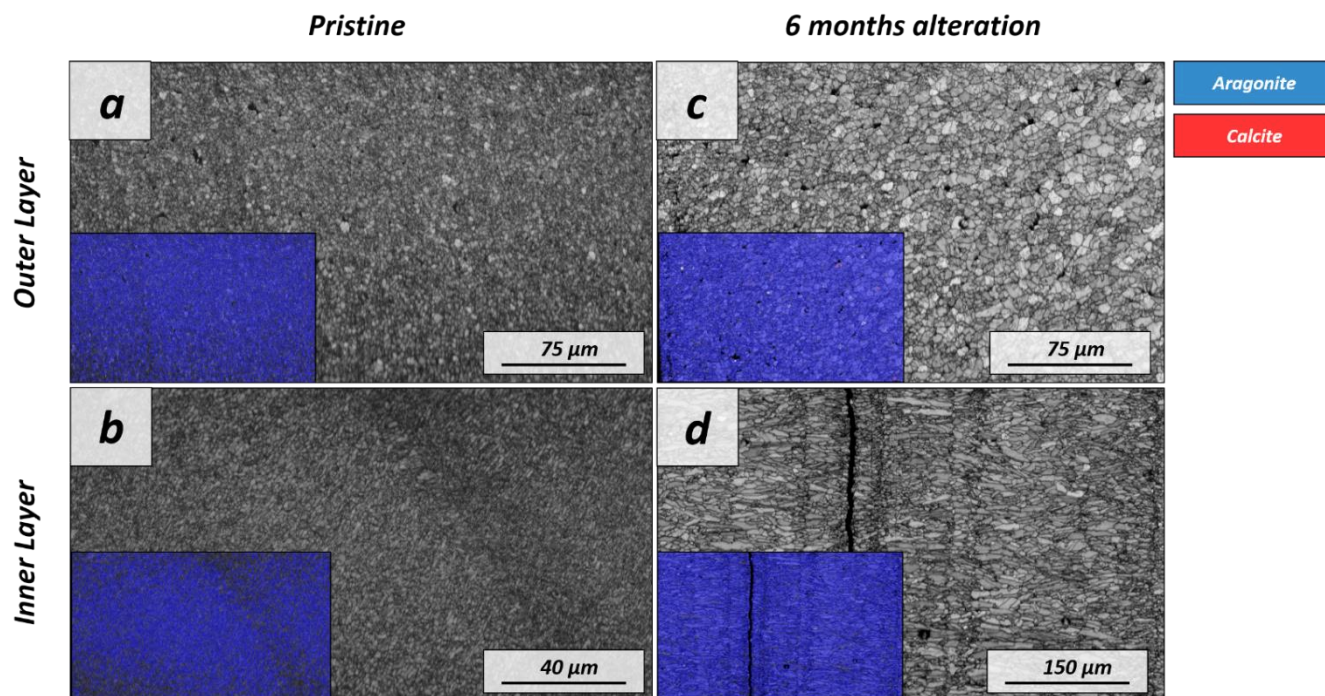


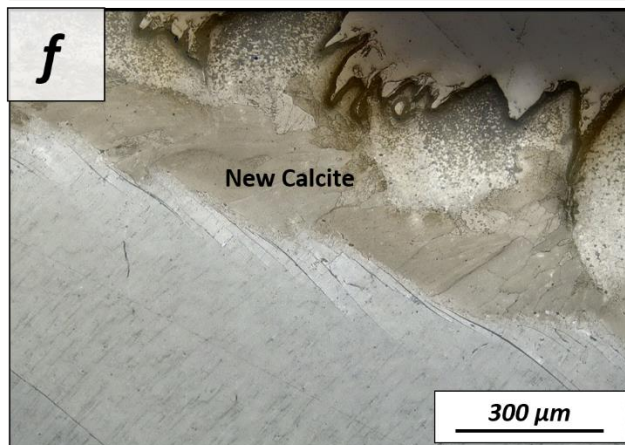
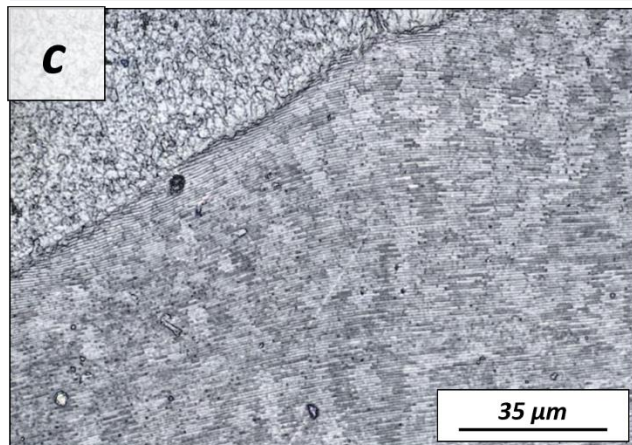
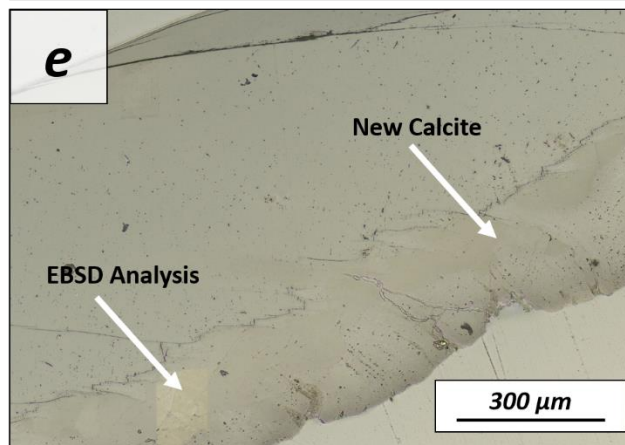
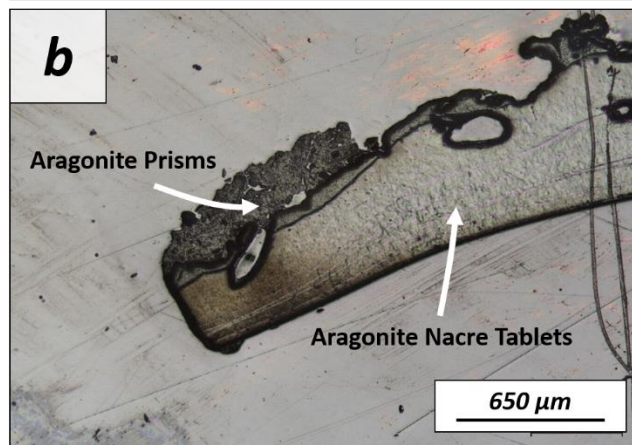
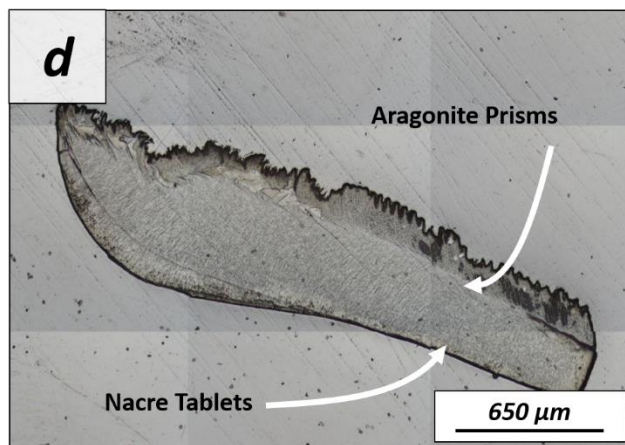
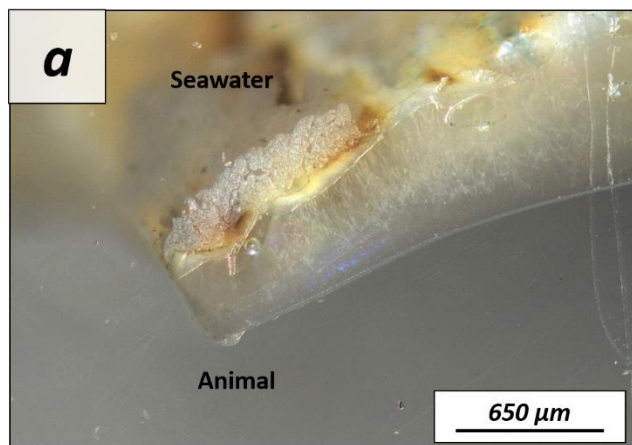
Figure A6. EBSD band contrast and phase maps illustrating the differences in the microstructure and mineralogy between the pristine and the most altered shell of *Arctica islandica* after 6 months of hydrothermal alteration with a Mg-rich, burial, fluid at 80°C. A phase change is not observable.

1060



Pristine

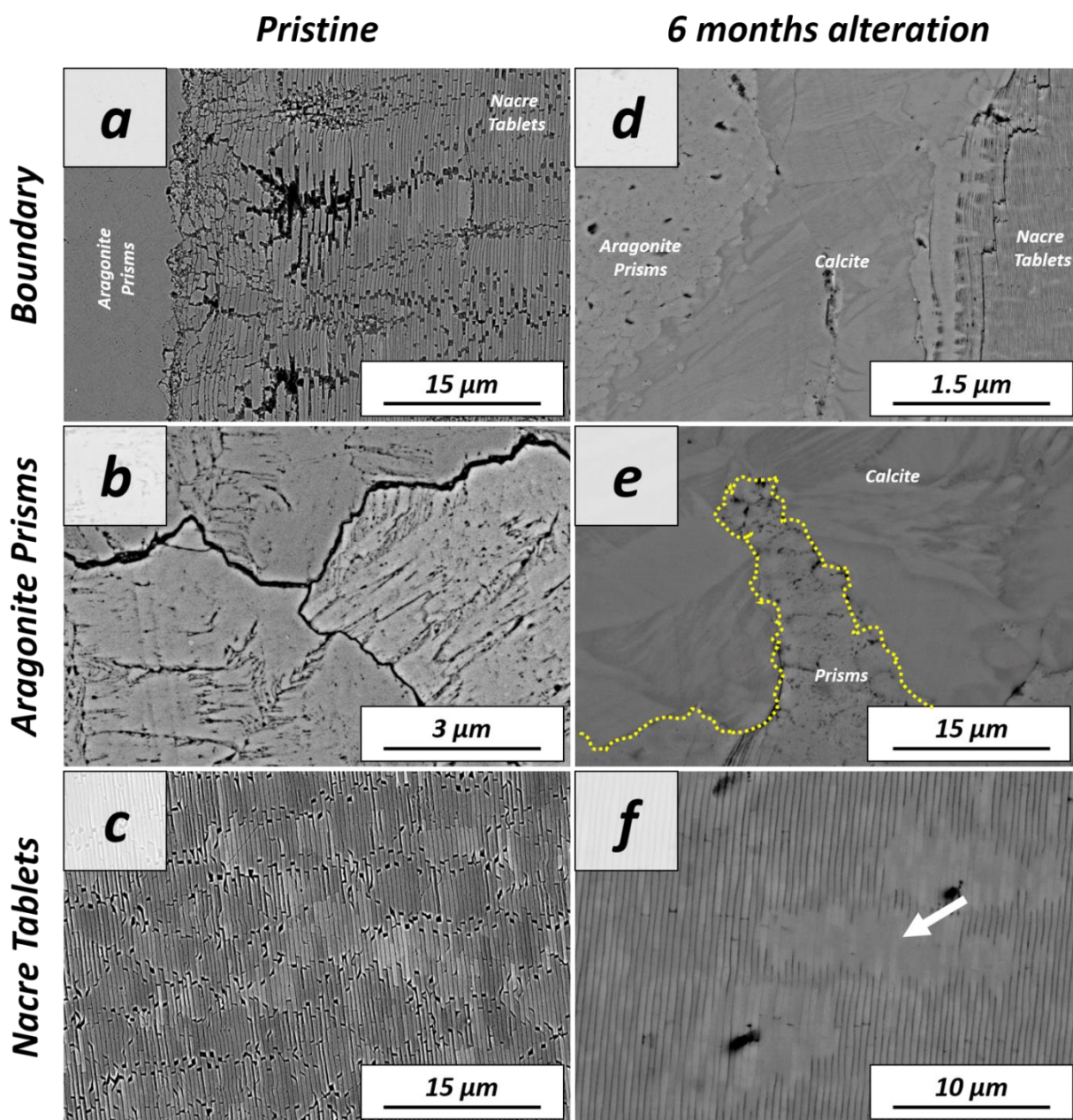
6 months alteration





1065

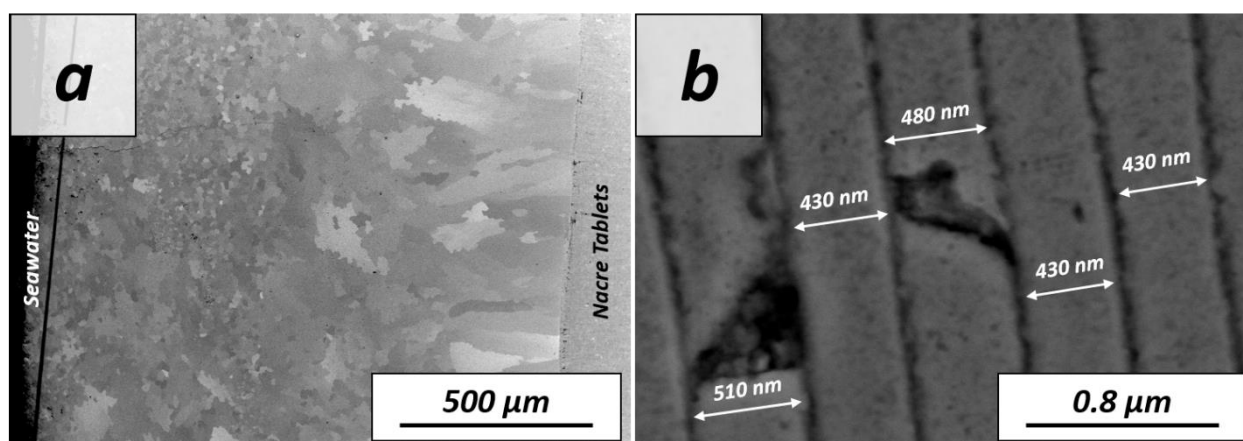
Figure A7. Laser confocal microscopy images of (a-c) pristine and (d-f) altered shells of *Haliotis ovina*. The shell is composed of two layers: a prismatic outer layer and a nacreous inner layer close to the animal soft tissue. While the nacreous layer shows no major structural change upon alteration, large calcite crystals can be observed in the prismatic layer after 6 months interaction with the burial, fluid.



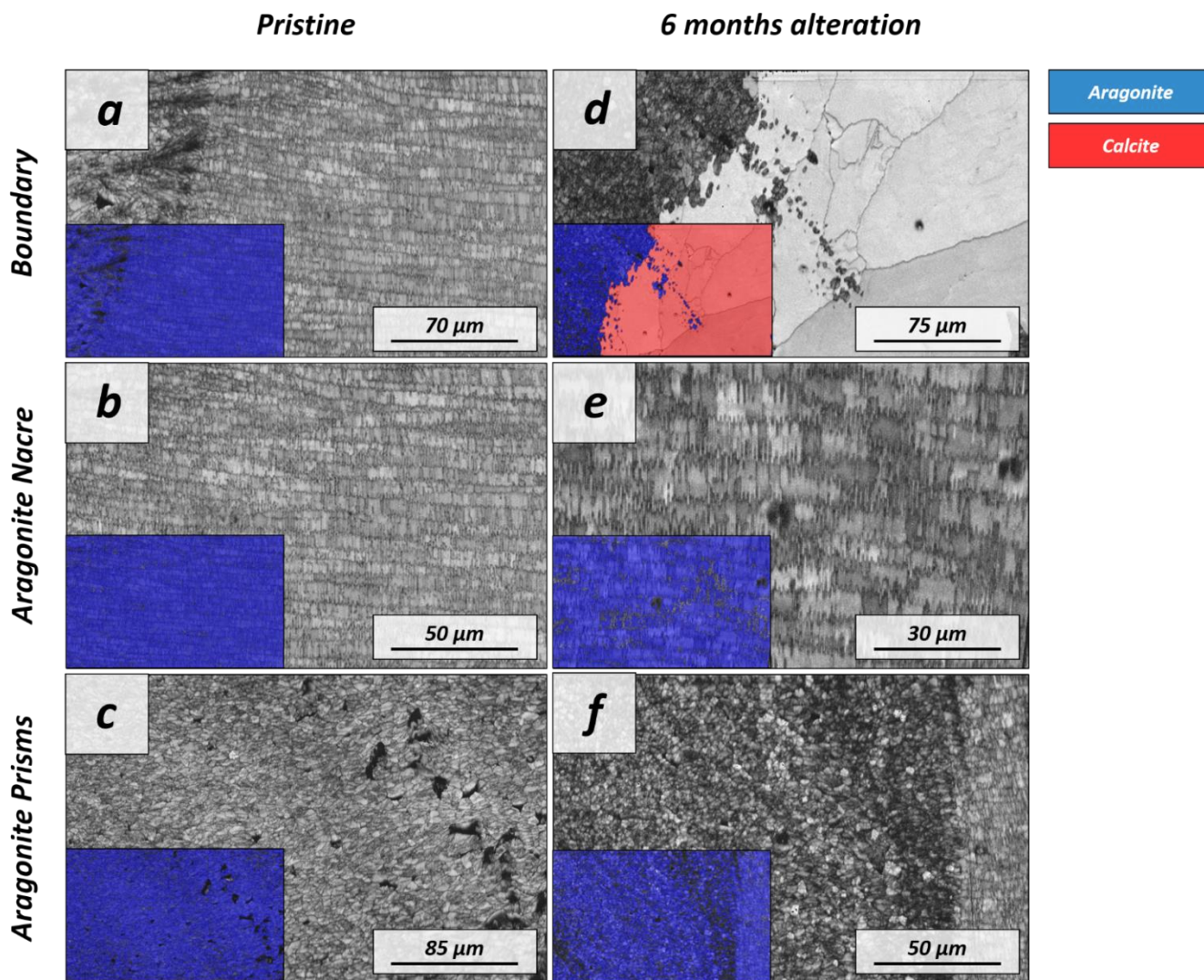


1070 **Figure A8.** FE-SEM images depicting the internal structure of (a,c) pristine and of (d-f) altered shells of the gastropod *Haliotis ovina*. (a) *Haliotis ovina* shells consist of two layers: (b) An outer layer formed of aragonite prisms up to 3 micrometres in width and (c) an inner layer next to the soft tissue of the animal consisting of columnar assemblies of nacre tablets. (d-f) Hydrothermal alteration of *Haliotis ovina* shells for 6 months at 80°C, in burial fluid leads to the formation of new calcite crystals in the prismatic layer. These calcite crystals are concentrated at the interphase between the prisms and the nacre tablets.

1075 The aragonitic nacre tablets do not show transformation into calcite. However, tablet amalgamation is well observable, clearly visible as the edges and margins within stacks of tablets become blurred (white arrow in Fig A8d).



1080 **Figure A9.** FE-SEM images showing the (a) prismatic and (b) nacreous layers of the shell of the gastropod *Haliotis ovina*. (a) Aragonitic prisms which build the outer layer of the shell are not similar in size. Small prisms form the outermost shell layers, while large prisms accumulate at the transition to the nacreous shell portion. (a, b) Aragonitic nacre tablet assemblies are next to the soft tissue of the animal. The tablets have a width in cross-section between 400 to 500 nm.



1085

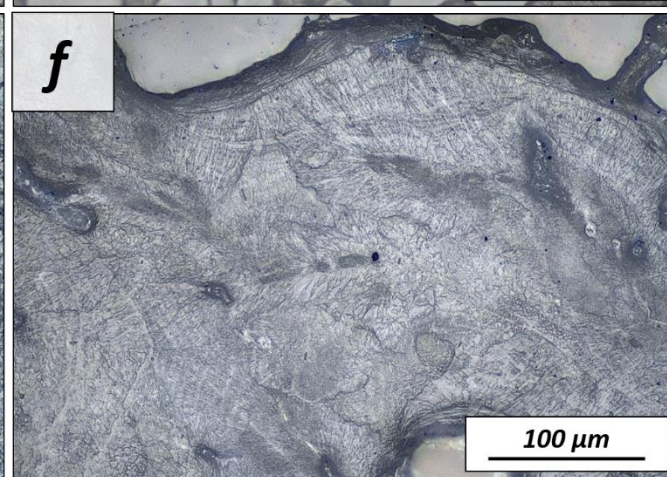
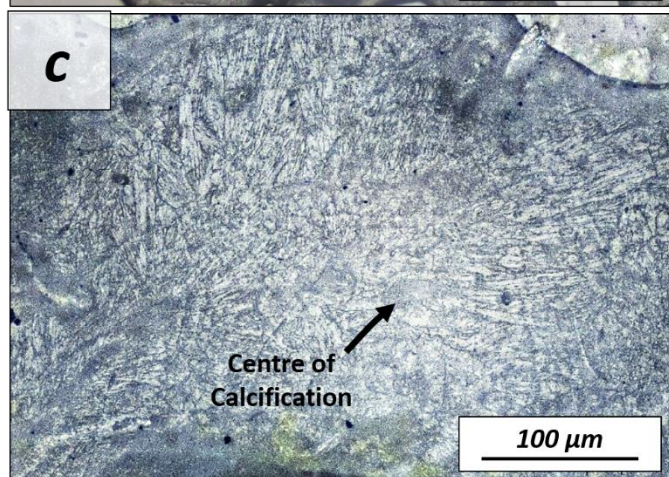
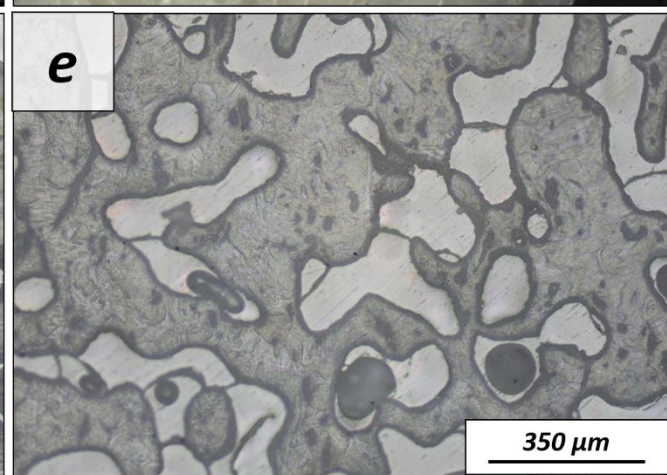
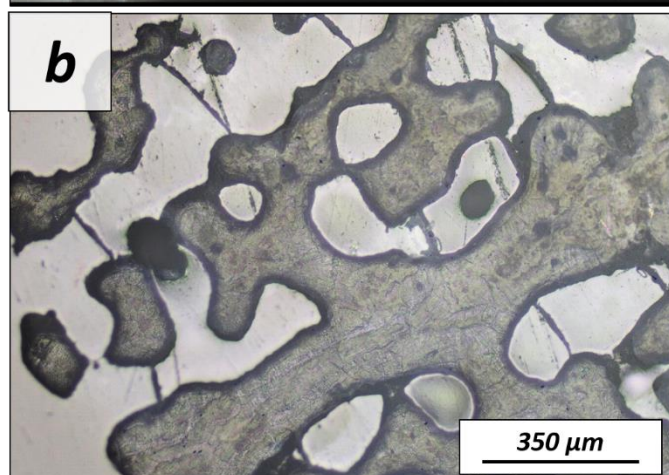
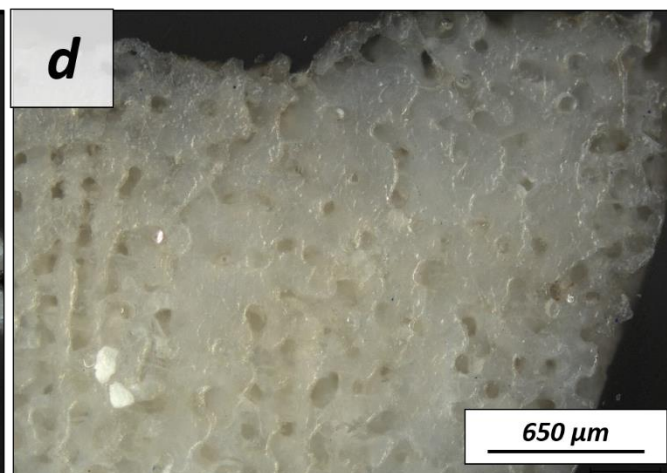
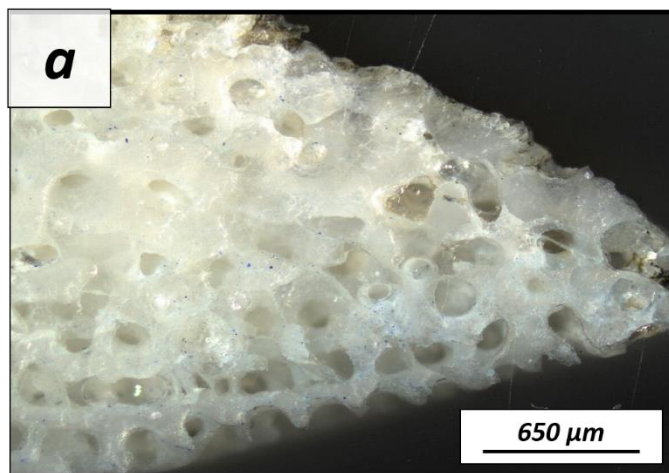
Figure A10. EBSD band contrast and phase maps illustrating differences in microstructure and mineralogy between the pristine and the most altered shells of *Haliotis ovina*; alteration lasted for 6 months and was done with a Mg-rich, burial, fluid at an alteration temperature of 80 °C. It is well visible that large parts of the prismatic layer are transformed to calcite, while the nacreous shell layer still consists solely of aragonite.

1090



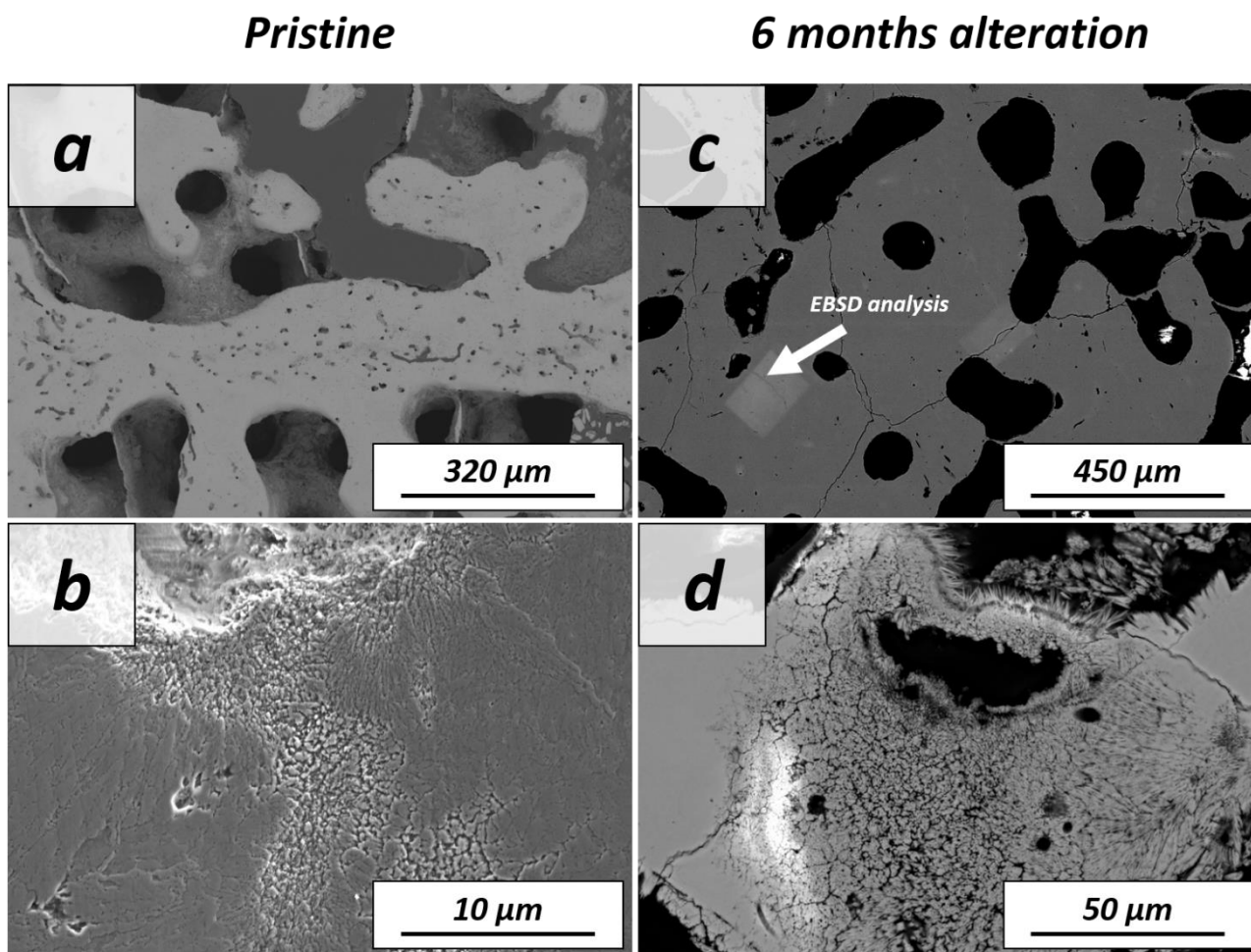
Pristine

6 months alteration





1095 **Figure A11.** Laser confocal microscopy images of: (a-c) the pristine and the (d-f) altered skeleton of *Porites* sp. This coral species has a huge primary porosity, while the aragonitic hard tissue itself is densely mineralized (a to c). Aragonite acicles, needles and fibrils grow out of centres of calcification (a). Hydrothermal alteration for 6 months, at 80 °C and in a Mg-rich fluid, does not induce significant changes to the skeleton microstructure, as visible in Figs. A11d to A11f.

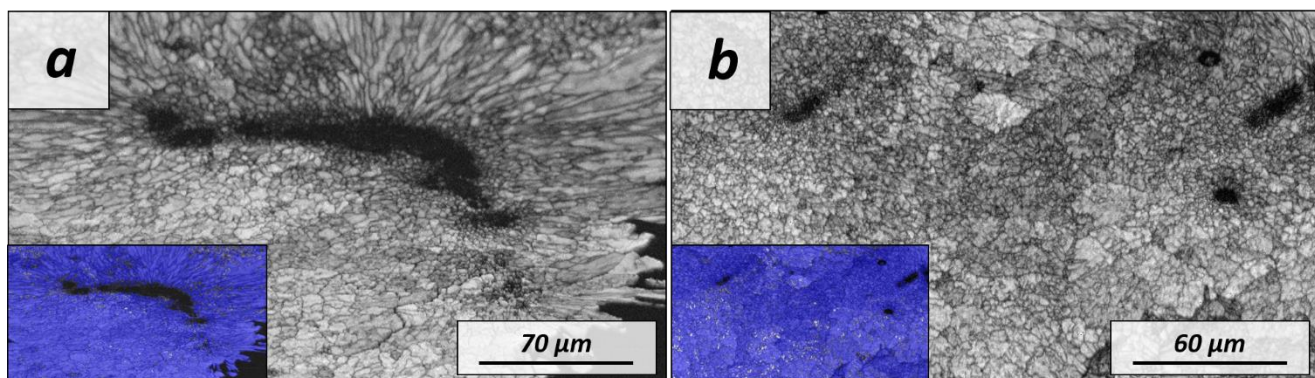


1100 **Figure A12.** SEM images showing the (a,b) pristine and (c,d) altered skeletons of the coral *Porites* sp. The stony skeleton of *Porites* sp. has abundant intrinsic porosity within the mineralized units. The aragonite grows as fibrils outward from the centres of calcification. (c,d) The aragonitic microstructure of the coral *Porites* sp. is extremely resistant and undergoes no major changes upon hydrothermal alteration with a burial-mimicking fluid for 6 months at 80°C according to SEM images.



Pristine

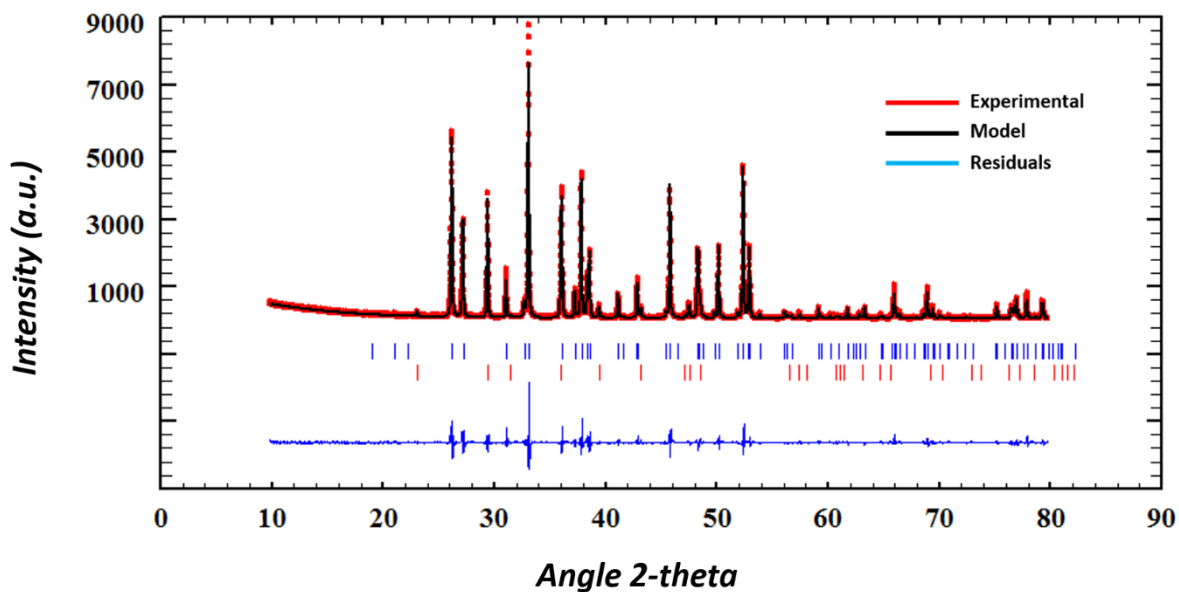
6 months alteration



1105

Figure A13. EBSD band contrast and phase maps illustrating the differences in microstructure and the mineralogy between the pristine and the most altered skeleton of *Porites* sp.

***Haliotis ovina* + 6 months interaction with Burial Fluid**



1110

Figure A14. Exemplary Rietveld refinement plot for an altered *Haliotis ovina* sample (6 months, 80 °C in Mg-rich fluid). Red dots: data points, black line: calculated XRD profile, bottom blue line: difference between observed and calculated data, blue vertical bars: positions of aragonite diffraction peaks, red vertical bars: position of calcite diffraction peaks.